Functional Roles of MMP14 and MMP15 in Early Postnatal Mammary Gland Development

Tamar Y. Feinberg[1,2,3] R. Grant Rowe[1±], Thomas L. Saunders[1,4] & Stephen J. Weiss[1,2,3*]

[1]Division of Molecular Medicine and Genetics, Department of Internal Medicine, [2]Life Sciences Institute, [3]Cellular and Molecular Biology Graduate Program, [4]Transgenic Animal Model Core, Biomedical Research Core Facilities, University of Michigan, Ann Arbor, MI 48109

Biological Sciences, Developmental Biology

*Corresponding Author:
Stephen J. Weiss, M.D.
University of Michigan
Life Sciences Institute
5000 LSI
210 Washtenaw
Ann Arbor, MI 48109-2216
Ph: 734-764-0030
Fax: 734-764-1934
Email: sjweiss@umich.edu

Keywords: morphogenesis, mammary gland, matrix metalloproteinases

±*R. Grant Rowe, M.D., Ph.D. current address is Pediatric Hematology-Oncology, Dana Farber Cancer Institute, Boston, MA 02215

ABSTRACT

During late embryogenesis, mammary epithelial cells initiate migration programs that drive ductal invasion into the surrounding adipose-rich mesenchyme. Currently, branching morphogenesis is thought to depend on the mobilization of the membrane-anchored matrix metalloproteinases, MT1-MMP/MMP14 and MT2-MMP/MMP15, that drive epithelial cell invasion by remodeling the extracellular matrix and triggering associated signaling cascades. However, the roles that these proteinases play during mammary gland development *in vivo* remain undefined. Herein, we characterize the impact of global *Mmp14* and *Mmp15* targeting on early postnatal mammary gland development. Unexpectedly, both *Mmp14*$^{-/-}$ and *Mmp15*$^{-/-}$ mammary glands retain the ability to generate intact ductal networks. Though neither proteinase is required for branching morphogenesis, transcriptome profiling reveals a key role for MMP14 and MMP15 in regulating mammary gland adipocyte differentiation. Whereas MMP14 promotes the generation of white fat depots critical for energy storage, MMP15 differentially controls the formation of thermogenic brown fat. Taken together, these data not only indicate that current paradigms relevant to proteinase-dependent morphogenesis need be revisited, but also identify new roles for the enzymes in regulating adipocyte fate determination in the developing mammary gland.

INTRODUCTION

During postnatal mammary gland development, epithelial ducts mount a cohesive cell invasion program that allows them to penetrate a periductal interstitial matrix populated by fibroblasts and a surrounding adipocyte-rich mesenchyme (Ewald et al., 2008; Ewald et al., 2012; Watson and Khaled, 2008). Similar to other epithelial organ systems, branching morphogenesis begins between gestation days E12 and E15 with the formation of primary buds that undergo reiterative branching into the underlying mesenchyme (Ewald et al., 2008; Ewald et al., 2012; Hogg et al., 1983; Watson and Khaled, 2008). Between E16 and E20, mammary epithelial cords give rise to polarized, bilayered tubules composed of inner-facing luminal epithelial cells and basal-oriented myoepithelial cells (Hogg et al., 1983; Sun et al., 2010). In tandem with epithelial development, the surrounding adipose-rich tissue, termed the mammary fat pad, likewise undergoes morphogenesis (Hovey and Aimo, 2010; Inman et al., 2015). Beginning during late gestation (i.e., E14 to E18) and continuing through early postnatal development, the fat pad is eventually dominated by committed adipocytes that support epithelial morphogenesis and tissue homeostasis (Wang et al., 2015). At birth, the mammary gland rudiment is a small, simply branched structure that is believed to lie dormant until the onset of puberty (~3 wks of age) (Ewald et al., 2008; Ewald et al., 2012; Hogg et al., 1983; Watson and Khaled, 2008).

Recent studies emphasize critical roles for proteolytic enzymes belonging to the matrix metalloproteinase (MMP) family in the tissue remodeling events that are activated during branching morphogenesis, with specific focus on two closely related membrane-anchored MMPs, termed MT1-MMP/MMP14 and MT2-MMP/MMP15 (Alcaraz et al., 2011; Bonnans et al., 2014; Mori et al., 2009; Mori et al., 2013; Rebustini et al., 2009; Weaver et al., 2014). Consistent with their >50% homology at the amino acid level, both MMP14 and MMP15 are capable of hydrolyzing a wide variety of substrates ranging from cell surface molecules and growth factors to extracellular matrix (ECM) components (Barbolina and Stack, 2008; Itoh, 2015; Rowe and Weiss, 2009). With particular regard to mammary gland morphogenesis, MMP14 has been reported to control branching events by both proteolytic mechanisms whereby epithelial cells dissolve confronting ECM barriers as well as proteinase-independent mechanisms by acting as a scaffolding hub for signal transduction cascades that control cell motility and cell sorting (Alcaraz et al., 2011; Mori et al., 2009; Mori et al., 2013; Simian et al., 2001; Weaver et al., 2014). Similarly, MMP15 has been reported to regulate branching morphogenesis and associated proliferative responses as a consequence of its ability to proteolytically remodel the basement membrane and regulate growth factor expression (Hotary et al., 2000; Rebustini et al., 2009). Nevertheless, conclusions regarding roles for MMP14 and MMP15 in branching morphogenesis largely derive from *in vitro* and *ex vivo*

models, and the roles that these enzymes play *in vivo* within the developing mammary gland remain undefined.

Herein, we describe a mammary gland branching program that occurs during the first 10 days of early postnatal development and gives rise to an organized network of polarized ductal structures that penetrate a mature adipocyte-populated stroma, offering a robust platform in which to characterize the protease-dependent and protease-independent roles of MMP14 and MMP15 *in vivo*. Using *Mmp14*$^{-/-}$ mice as well as a newly generated *Mmp15*$^{-/-}$ mouse line, we provide the first full-scale analysis of the differential functions of these MT-MMPs in early postnatal mammary gland development.

RESULTS

Early postnatal morphogenesis of the developing mouse mammary gland.

At birth (i.e., postnatal day 0; P0), mammary gland rudiments of female mice appear as primitive ductal trees whose ill-defined branches are found immediately adjacent to the nipple (Fig. 1A,B). In H&E stained cross-sections, the mammary epithelium is shown to be organized into cohesive structures containing a mixture of solid cords and hollow ducts (Fig. 1C). Immunohistochemical analyses further reveal that epithelial structures are dominated by cells expressing the luminal marker, cytokeratin 8 (CK8), with only low levels of cytokeratin 18 (CK18), in tandem with a heterogeneous distribution of cells expressing the basal marker, cytokeratin 14 (CK14) and the absence of cytokeratin 5 (CK5) (Fig. 1D) (Ewald et al., 2008; Ewald et al., 2012; Sun et al., 2010; Watson and Khaled, 2008). Epithelial cells expressing the myoepithelial marker, α-smooth muscle actin (αSMA) (Ewald et al., 2008; Ewald et al., 2012; Hogg et al., 1983; Watson and Khaled, 2008), are confined to the basal compartment, but in a scattered fashion that outlines the rudiments (Fig. 1D). In marked contrast, between P5 and P10, the mammary gland undergoes a morphogenic program wherein an established network of hollow ducts extend their length through the surrounding mesenchyme by 2-fold while branch number increases 3-fold and the surface area covered by ductal structures expands 4-fold (Fig. 1A-C). Coincident with this maturation process, both CK8 and CK18 expression are up-regulated in the luminal compartment while CK14 is confined primarily to basal epithelial cells in association with the continuous circumferential expression of αSMA (Fig. 1D). This early developmental program coincides with epithelial cell proliferation, as evidenced by Ki67 expression in the CK8-positive compartment at P0 as well as P5 (Fig. S1A-B). These changes in epithelial cell and ductal tree organization are complemented by striking changes in the mammary gland fat pad wherein small lipid-laden adipocyte/adipocyte precursors mature into large, unilocular adipocytes (Fig. 1C). While the P0-P10 mammary ducts are consistently invested by a laminin- and type IV collagen- rich basement membrane (Fig. 1E), a periductal network of organized type I collagen fibrils does not fully develop until P5-P10 (Fig. 1F). Hence, during the early postnatal period, both the mammary epithelia and stroma activate a morphogenetic program that generates a well-organized network of ductules that predate those more frequently associated with pubertal development (Huebner and Ewald, 2014; Inman et al., 2015; Macias and Hinck, 2012; Watson and Khaled, 2008).

MMP14 dependent regulation of branching morphogenesis: *In vitro* versus *in vivo*.

Based largely on *in vitro* evidence, MMP14 has been proposed to regulate branching morphogenesis by both proteinase- dependent and independent mechanisms (Alcaraz et al., 2011; Mori et al., 2009; Mori et al., 2013; Weaver et al., 2014). Using *Mmp14*$^{lacZ/+}$ mice (Yana et al., 2007), β-galactosidase activity is detected in the branching ductal tree as well as the

surrounding mesenchyme at birth and P5 (Fig. 2A). By P10, LacZ-expressing cells delineate and circumscribe the entire neonatal mammary gland, from the ducts closest to the nipple to their terminal ends (Fig. 2A) with cross-sections highlighting MMP14 expression in luminal epithelial cells and myoepithelial cells as well as the surrounding stroma (Fig. 2B). LacZ expression also correlates with an increase in *Mmp14* levels in the developing mammary tissue (Fig. 2C).

To first assess the role of mammary epithelial cell-derived MMP14 *in vitro*, $Mmp14^{lacZ/+}$ mammary epithelial organoids were embedded in 3-dimensional (3-D) type I collagen hydrogels (Chun et al., 2004; Haslam et al., 2008; Sabeh et al., 2009; Simian et al., 2001). As shown, *Mmp14* is expressed both at time 0 and during the formation of an arborized branching network generated in the presence of FGF-2 after a 5 d culture period (Fig. 2D) (Haslam et al., 2008; Simian et al., 2001). Consistent with the premise that MMPs are able to drive type I collagen-invasive activity (Alcaraz et al., 2011; Chun et al., 2004; Mori et al., 2009; Mori et al., 2013; Sabeh et al., 2009; Simian et al., 2001; Tang et al., 2013; Weaver et al., 2014), branching morphogenesis is inhibited completely when organoids are cultured in the presence of the pan-specific MMP inhibitor, BB-94 (Chun et al., 2004; Sabeh et al., 2009) (Fig. 2E). More importantly, organoids recovered from MMP14-deleted mice display a complete loss of branching activity (Fig. 2E), a result consistent with MMP14's role as the dominant pericellular type I collagenase operative in mammalian cells (Chun et al., 2004; Rowe and Weiss, 2009; Sabeh et al., 2009; Tang et al., 2013). Nevertheless, an MMP14-dependent block in branching morphogenesis through native type I collagen matrices could also result from protease-independent effects on epithelial cell sorting, motility or metabolism (Mori et al., 2009; Mori et al., 2013; Sakamoto et al., 2014). As such, $Mmp14^{+/+}$ and $Mmp14^{-/-}$ mammary epithelial organoids were alternatively embedded in 3-D hydrogels of Matrigel (Ewald et al., 2008; Ewald et al., 2012; Lo et al., 2012), a mixture of basement membrane-associated proteins whose proteolytic remodeling is not required to support cell invasion programs (Rowe and Weiss, 2008). As reported previously (Ewald et al., 2008; Ewald et al., 2012; Lo et al., 2012), wild-type mammary organoids embedded in Matrigel hydrogels form budding lobular structures in response to FGF-2-mediated signaling (Fig. 2F). Inconsistent, however, with the contention that MMP14 regulates morphogenesis via proteinase-independent mechanisms (Mori et al., 2009; Mori et al., 2013), neither Matrigel-embedded organoids cultured in the presence of BB-94 nor organoids recovered from $Mmp14^{-/-}$ mice display defects in branching activity (Fig. 2F). Hence, in the presence of a permissive ECM environment, MMPs are not required to support morphogenic programs.

While *in vitro* models provide useful tools for dissecting structure/function relationships, mounting evidence suggests that isolated epithelial cell-based model systems are unlikely to recapitulate the morphogenic programs occurring *in vivo* where the functional properties of

the surrounding mesenchyme play active roles in branching (Nelson and Larsen, 2015; Varner and Nelson, 2014). As such, we next sought to directly assess requirements for MMP14 during mammary gland morphogenesis *in vivo.* Though the morbid status of *Mmp14*$^{-/-}$ mice and their failure to undergo sexual maturation preclude efforts to analyze late stage mammary gland development (Holmbeck et al., 1999; Zhou et al., 2000), the newly described P0-P10 program potentially provides a unique window of opportunity for such analyses. Interestingly, mammary glands harvested from P0 *Mmp14*$^{-/-}$ mice generate branching ductal networks comparable to those of wild-type and *Mmp14*$^{+/-}$ littermates as visualized by whole mount carmine staining and quantified by ductal length and branch point number (Fig. 3A,B). More remarkably, at P5 and P10, *Mmp14*$^{-/-}$ mice mount a mammary gland branching program similar, if not identical, to those observed in *Mmp14*$^{+/+}$ or *Mmp14*$^{+/-}$ littermates (Fig. 3C-F). Further, immunohistologic assessments of *Mmp14*$^{-/-}$ mammary gland sections revealed no differences in the expression or organization of CK18, CK14 or α-SMA from P0 through P10 (Fig. 4A,B). Likewise, epithelial cell organization, as assessed by the apical distribution of the tight junction protein, zonula occludens (ZO)-1, or the adherens junction marker, E-cadherin (Ewald et al., 2008; Ewald et al., 2012; Inman et al., 2015), is indistinguishable between *Mmp14*$^{+/+}$, *Mmp14*$^{+/-}$ or *Mmp14*$^{-/-}$ mice at P10 (Fig. 4B). While MMP14 has previously been implicated in the proliferation-associated signaling cascades that drive branching morphogenesis (Gutierrez-Fernandez et al., 2015; Riggins et al., 2010), neither Ki67 expression, TUNEL staining nor senescence are affected in *Mmp14*$^{-/-}$ glands (Fig. 4C,D). Finally, deleting MMP14 did not discernably alter basement membrane or interstitial matrix assembly, respectively, as reflected in comparable type IV collagen and laminin staining (Fig. 4E) or levels of type I collagen as assessed by immunofluorescence and Sirius Red staining (Fig. 4F).

Neonatal mammary gland branching morphogenesis also coincides with the increased expression of two secreted members of the MMP gene family that have been previously implicated in mammary gland branching and development, i.e., *Gelatinase A/Mmp2* and *Stromelysin-1/Mmp3* (Correia et al., 2013; Kessenbrock et al., 2013; Lochter et al., 1997; Wiseman et al., 2003; Witty et al., 1995) (Fig. S2A,C). Further, MMP14 can activate MMP2 *in vivo,* a proteinase thought to mediate MMP14 function and compensate partially for *Mmp14* deficiency (Itoh, 2015; Oh et al., 2004). Nevertheless, as previously described (Wiseman et al., 2003), *Mmp2*$^{-/-}$ mammary glands develop comparable branching structures relative to those of littermate controls in pre-pubertal mice (Fig. S2B) . Further, while recent reports have identified critical protease-dependent as well as protease-independent roles for MMP3 in mammary gland development (Correia et al., 2013; Kessenbrock et al., 2013; Lochter et al., 1997; Wiseman et al., 2003; Witty et al., 1995), *Mmp3*$^{-/-}$ mammary glands establish branching structures that are comparable in length and complexity to those of *Mmp3*$^{+/+}$ and *Mmp3*$^{+/-}$

littermates with normal distribution of luminal epithelial and myoepithelial cell populations (Fig. S2D,E).

Neonatal mammary gland branching proceeds in the absence of MMP15.

Membrane-anchored MMP15 is structurally related to MMP14, enriched in the mammary epithelium (Szabova et al., 2005), and has recently been implicated in branching morphogenesis ex vivo (Rebustini et al., 2009). Using *Mmp15*^{lacZ} knock-in mice (Fig. 5A), *Mmp15* expression can be detected throughout the mammary epithelial cell compartment at birth as well as through P10 (Fig. 5B,C), a result further corroborated by up-regulated *Mmp15* levels during this period (Fig. 5D). *Mmp15*-targeted mice were therefore employed to address the requirement for *Mmp15* in branching morphogenesis wherein exons 4 and 5 of the catalytic domain were flanked by loxP sites (Fig. S3A), and deleted by breeding *Mmp15*$^{flox/flox}$ mice with EIIA-Cre mice. Crosses between *Mmp15*$^{+/-}$ mice generated *Mmp15*$^{+/+}$, *Mmp15*$^{+/-}$ and *Mmp15*$^{-/-}$ mice in normal Mendelian ratios, yielding a total of 68 *Mmp15*$^{+/+}$, 146 *Mmp15*$^{+/-}$ and 70 *Mmp15*$^{-/-}$ mice in 284 total offspring; and *Mmp15*$^{-/-}$ mice remained similarly viable throughout adulthood. Importantly, germline deletion of *Mmp15* did not affect *Mmp14* expression (Fig. 5E), ruling out any compensatory interactions between these closely related MMP family members.

In vivo assessments of *Mmp15*$^{+/+}$, *Mmp15*$^{+/-}$ and *Mmp15*$^{-/-}$ mammary glands revealed correspondingly similar branching structures as assessed by whole mount carmine staining at birth as well as P10 and quantified by ductal penetration or total branch points(Fig. 5F-I). Similarly, explanted *Mmp15*$^{-/-}$ and *Mmp15*$^{+/+}$ mammary epithelial cell organoids in 3-D type I collagen or Matrigel mounted comparable *in vitro* branching programs (Fig. 5J,K). Further, as observed in *Mmp14*$^{-/-}$ mice, *Mmp15*$^{-/-}$ mammary epithelial ducts display an unaltered pattern of CK18, CK14, αSMA and E-cadherin expression (Fig S3B-D). While MMP15 has been reported to regulate the proliferative and apoptotic responses required for epithelial morphogenesis (Abraham et al., 2005; Rebustini et al., 2009), Ki67 levels are unchanged in the absence of *Mmp15* with apoptosis assessments revealing no significant differences across genotypes (Fig. S3E). Similarly, though MMP15 has been identified as a critical basement membrane remodeling enzyme during branching morphogenesis *ex vivo* (Rebustini et al., 2009) and a type I collagenolytic enzyme *in vitro* (Chun et al., 2004; Hotary et al., 2000), neither type IV collagen, laminin nor type I collagen levels are affected in the absence of *Mmp15* (Fig. S2F).

Differential roles for MMP14 and MMP15 in mammary gland development.

In order to probe for unanticipated functional roles of MMP14 and MMP15 in the early postnatal mammary gland in an unbiased fashion, we analyzed the transcriptome of the ductal networks and associated stroma in wild-type versus null mice. In *Mmp14*$^{-/-}$ mice, gene expression profiling revealed >250 differentially expressed genes relative to *Mmp14*$^{+/+}$ mammary tissue (using a 2-fold enrichment cutoff), with functional annotation clusters bridging 16 different gene ontology (GO) categories, including many associated with the epithelial cell compartment, such as cell adhesion, endocytosis, responses to endogenous stimuli, and G protein-coupled signaling cascades (DAVID Bioinformatics Resource, NIH, p-value/Ease < 0.05; Fig. 6A). Of note, gene expression profiling did not uncover significant changes in the proliferation- or senescence- associated signaling cascades highlighted in earlier work (Gutierrez-Fernandez et al., 2015; Riggins et al., 2010), despite undetectable levels of *Mmp14* in *Mmp14*$^{-/-}$ mammary gland tissue. However, given the number of genes associated with epithelial cell adhesion complexes and cytoskeletal organization [e.g., *Calmin*, *Plakophilin* 2, *Folliculin;* (Arimoto et al., 2014; Khabibullin et al., 2014; Loo et al., 2013)] , we examined mammary ducts recovered from P10 *Mmp14*$^{+/+}$ and *Mmp14*$^{-/-}$ mice by transmission electron microscopy (TEM). Interestingly, *Mmp14*$^{-/-}$ ducts form more intimate cell-cell junctions with a marked increase in the number of apical microvilli (Fig. S4A,B). By contrast, the transcriptome of *Mmp15*$^{-/-}$ mammary tissues uncovered only ~30 differentially expressed genes whose classification lacked any major associations with mammary epithelium-related GO categories (Fig. S5A). Accordingly, TEM analyses of *Mmp15*$^{-/-}$ ducts appear normal (Fig. S5B,C). Hence, while these data confirm active roles for MMP14 and MMP15 in early postnatal mammary gland development, the transcriptional changes recorded do not significantly impact on the ability of the organizing ductal network to penetrate the surrounding mesenchymal tissues.

Independent of the roles played by MMP14 or MMP15 in the mammary gland epithelial compartment, analyses of differentially expressed transcript profiles indicate that both MT-MMPs exert more significant effects on the developing mammary gland stroma. In *Mmp14*$^{-/-}$ mice, the down-regulated GO categories with the highest enrichment scores are tightly linked with the mammary gland stromal fat pad, with decreased expression of multiple transcripts associated with sterol metabolism, lipid biosynthesis, fatty acid metabolism and adipocyte maturation (Fig. 6B). In tandem with these changes, mammary gland adipocytes display a marked 2-fold decrease in overall size, as evidenced by H & E staining and TEM analyses as well as quantified by mean adipocyte diameter (43.3 μm ± 1.01 μm in *Mmp14*$^{+/+}$ mammary glands versus 22.8 μm ± 1.60 μm in *Mmp14*$^{-/-}$ glands (n=3 per genotype, p=0.0004)) (Fig. 6C; Fig. S6A). In an almost diametrically opposed fashion, the metabolic genes repressed in *Mmp14*$^{-/-}$ tissue are either upregulated or unchanged in *Mmp15*-targeted mice as most clearly evidenced by the differential expression of the adipokine, *Leptin* (Fig. 6D), an adipocyte-

derived secreted molecule responsible for regulating tissue metabolism and energy homeostasis (Wang et al., 2015; Wu et al., 2013). Unexpectedly, transcriptome analysis of *Mmp15*$^{-/-}$ mammary tissue further reveals a marked *increase* in a core suite of positive regulators of brown or induced brown (beige) adipocytes (Fig. S5A) – thermogenic adipocytes that can be identified based on their restricted expression of uncoupling protein-1 (UCP1) (Wang et al., 2015; Wu et al., 2013). Indeed, whereas adipocyte size is unaffected in many regions of the *Mmp15*$^{-/-}$ mammary glands, large clusters of small, multilocular adipocytes – the hallmark of beige/brown fat – are found throughout the knockout tissues in 4 of 6 animals characterized (Fig. 6E; Fig. S6B). As confirmed by qPCR, *Mmp15*$^{-/-}$ mammary tissues display a 4-to-5-fold increase in *Ucp1* transcript levels as well as increased expression of multiple genes required for mitochondrial biogenesis, adipocyte thermogenesis and *Ucp1* induction, including *Dio2*, *Fabp3*, *Prdm16* and *Pgc1α* (Cohen et al., 2014; Marsili et al., 2011; Vergnes et al., 2011; Wu et al., 2013) (Fig. 6F). Further, cross-sections of *Mmp15*$^{-/-}$ mammary glands document increased UCP1 protein levels as well as a marked increase in mitochondrial number, size and cristae (Fig. 6G; Fig. S6C-E), hallmarks of beige/brown adipocytes (Gouon-Evans and Pollard, 2002; Harms et al., 2014; Liesa and Shirihai, 2013). Finally, corroborating the divergent roles of MMP14 and MMP15 in mammary fat pad development, brown/beige-associated transcripts or protein levels remain unchanged or are markedly reduced in *Mmp14*$^{-/-}$ glands (Fig. 6G,H). Hence, while MMP14 promotes white fat-associated adipogenesis in the developing mammary gland, MMP15 alternatively serves as an endogenous suppressor of beige/brown fat production.

DISCUSSION

MMP14 and MMP15 have been reported to play diverse roles in a range of morphogenesis-associated processes, including cell adhesion and motility, invasion, proliferation, energy metabolism, senescence, the proteolytic processing of growth factors, cytokines and chemokines as well as ECM remodeling (Ager et al., 2015; Alcaraz et al., 2011; Barbolina and Stack, 2008; Bonnans et al., 2014; Chun et al., 2004; Fahlman et al., 2014; Fu et al., 2013; Itoh, 2015; Kajita et al., 2001; Koshikawa et al., 2000; Koziol et al., 2012; Mori et al., 2009; Mori et al., 2013; Rebustini et al., 2009; Sabeh et al., 2009; Sakamoto et al., 2014; Shimizu-Hirota et al., 2012; Simian et al., 2001; Tang et al., 2013; Taylor et al., 2015; Weaver et al., 2014; Yana et al., 2007). Consistent, in part, with previous reports linking MT-MMPs with epithelial cell branching programs (Alcaraz et al., 2011; Bonnans et al., 2014; Mori et al., 2009; Mori et al., 2013; Rebustini et al., 2009; Weaver et al., 2014), we find that MMP14, but not MMP15, is required for mammary epithelial organoid branching through type I collagen barriers *in vitro*. However, in contrast to earlier findings (Mori et al., 2009), we find that MMP14-expressing mammary epithelial cells in 3D culture lack a competitive sorting advantage relative to MMP14-null epithelial cells and are instead distributed throughout the branching networks. Further, when *Mmp14*$^{-/-}$ or *Mmp15*$^{-/-}$ epithelial organoids are embedded in Matrigel (Ewald et al., 2008; Ewald et al., 2012; Lo et al., 2012), morphogenesis proceeds in an unperturbed fashion – even in the presence of a pan-specific MMP inhibitor. Given these divergent outcomes, and the inability of model systems to recapitulate mammary gland architecture or stromal cell interactions (Nelson and Larsen, 2015), we turned to the *in vivo* setting.

Unlike *in vitro* culture conditions, primordial mouse mammary ducts are encased in a coat of type IV collagen and laminin that is surrounded by low levels of type I collagen. Nevertheless, given the broad substrate repertoire of MMP14 and the multiple biological activities that have been assigned to its functions (Ager et al., 2015; Alcaraz et al., 2011; Barbolina and Stack, 2008; Bonnans et al., 2014; Chun et al., 2004; Fahlman et al., 2014; Fu et al., 2013; Itoh, 2015; Kajita et al., 2001; Koshikawa et al., 2000; Koziol et al., 2012; Mori et al., 2009; Mori et al., 2013; Rebustini et al., 2009; Rowe and Weiss, 2009; Sabeh et al., 2009; Sakamoto et al., 2014; Shimizu-Hirota et al., 2012; Simian et al., 2001; Tang et al., 2013; Taylor et al., 2015; Weaver et al., 2014; Yana et al., 2007), we were surprised to find that deleting the proteinase *in vivo* exerted little, if any, effect on morphogenesis. Likewise, despite an *ex vivo* requirement for MMP15 in submandibular gland proliferation, matrix remodeling and branching (Rebustini et al., 2009), mammary glands from *Mmp15*-targeted mice assembled normal ductal networks through P10. Taken together, the overall similarities of the ductal networks generated in *Mmp14*$^{-/-}$ or *Mmp15*$^{-/-}$ mice suggest that any *in vivo* defects related to tissue-invasive activity or branching are, at best, subtle. Of note, a small cohort of

the *Mmp14*$^{-/-}$ mice (i.e., 3 of 15 total) displayed an unusually reduced body size with partial mammary gland defects noted at P10 (i.e., mammary ducts branched comparably, but appeared more primitive in their architecture). However, given the reduced feeding of this cohort and the known influence of nutrient deprivation on tissue morphogenesis (Londhe et al., 2013), we did not include these animals in our analyses.

Despite the retention of intact mammary gland branching programs in *Mmp14*$^{-/-}$ or *Mmp15*$^{-/-}$ mice, we did not directly rule out a potential compensatory role for *Mmp14* and *Mmp15* in postnatal morphogenesis. As *Mmp14/Mmp15* double-null mice die during embryogenesis (Szabova et al., 2010), we alternatively targeted both proteinases selectively in the mammary epithelial compartment, but these analyses demonstrated that branching morphogenesis nevertheless proceeds in a normal fashion from birth through adulthood (submitted). Interestingly, a double knockout system was recently employed to target *Mmp14* and *Mmp15* in postnatal mice wherein mammary gland involution was unaffected (Szabova et al., 2010), suggesting that adult mammary tissue remodeling likewise proceeds in a MT-MMP-independent fashion. While MMP14 and MMP15 have previously been shown to endow neoplastic cells with the ability to degrade basement membrane (BM) barriers (Ota et al., 2009), it should be stressed that there is no evidence that mammary epithelial cells dissolve their underlying BM during morphogenesis *in vivo.* Indeed, during postnatal development, mammary epithelial cells remain separated from the periductal type I collagen meshwork by a patent BM (Ewald et al., 2008; Ewald et al., 2012; Williams and Daniel, 1983). More recently, Yamada and colleagues concluded that basement membranes undergo proteolytic remodeling during branching morphogenesis *ex vivo* (Harunaga et al., 2014), but efforts to implicate MMPs in this process were confined to the use of synthetic inhibitors that not only target all MMPs, but also ADAM/ADAM-TS family members that play critical roles in morphogenesis (Rowe and Weiss, 2009). Further, contrary to the conclusion that MMPs participate directly in BM proteolysis, TIMP-2, a potent endogenous MMP inhibitor (Chun et al., 2004; Sabeh et al., 2009), did not affect BM remodeling in their studies (Harunaga et al., 2014). Finally, we note that the early postnatal branching programs tracked in our studies were not mediated by other MMP family members implicated in later stages of development, including *Mmp2* or *Mmp3* (Correia et al., 2013; Kessenbrock et al., 2013; Wiseman et al., 2003). While recent work has also identified critical roles for MMP9 and MMP11 in mammary gland branching after the onset of puberty, both *Mmp9*$^{-/-}$ and *Mmp11*$^{-/-}$ mammary glands undergo normal pre-pubertal branching (Tan et al., 2014; Ucar et al., 2010; Wiseman et al., 2003).

Given the paucity of obvious structural defects in ductal morphogenesis found in *Mmp14*$^{-/-}$ or *Mmp15*$^{-/-}$ mice, we alternatively interrogated the mammary gland transcriptomes of the knockout tissues. Though MMP14 and MMP15 share considerable structural homology

(Itoh, 2015), effects on mammary gland gene expression were notably distinct. For example, *Mmp14*$^{-/-}$, but not *Mmp15*$^{-/-}$, mammary glands display increased expression of a number of cell adhesion/cytoskeleton-associated transcripts with *Mmp14*$^{-/-}$ ducts displaying changes in epithelial cell-cell junctions and the number of apical microvilli. While further work will be needed to define the functional consequences of these changes, the observed structural alterations highlight the fact that MMP14 does, in fact, affect mammary gland development, but not in a fashion that impacts branching-associated programs per se. In contrast with the epithelial cell-associated gene changes observed in *Mmp14*$^{-/-}$ mammary glands, the effects of deleting *Mmp15* were subtle with only a small subset of genes affected. We are, however, unable to assess catalytic activity of MMP15 per se as specific antibodies capable of distinguishing between the pro- and active forms of the enzyme have not been generated. Nevertheless, it is intriguing that the breast cancer-associated transcripts, *γ-synuclein* (Ahmad et al., 2007) and *Peroxiredoxin 2* (Stresing et al., 2013), are among the most significantly affected (i.e., ~5-fold increase and ~7-fold decrease, respectively).

In the mammary gland, the adipocyte-rich stroma plays important roles in regulating morphogenetic responses (Hovey and Aimo, 2010; Inman et al., 2015). Intriguingly, early in postnatal life, the mammary gland-associated pool of adipocytes contains both white and brown/beige fat (Gouon-Evans and Pollard, 2002; Master et al., 2002), but the factors that control their differential expression have not been defined previously. Independent of the effects of MMP14 and MMP15 on mammary epithelial cells, their more global and differential effects on mammary fat pad development were unanticipated. *Mmp14* targeting alone triggers a widespread down-regulation of transcripts associated with adipogenesis (Wang et al., 2015). By contrast, an *Mmp15*-null status exerts little effect on white fat development, but instead strongly enhances the formation of brown and/or beige fat as evidenced by the increased expression of a cohort of thermogenic genes (Wu et al., 2013). Our lab has previously established roles for MMP14 in coordinating adipocyte maturation *in vivo*, as evidenced by the aborted white adipose tissue development in the dermal and inguinal adipose tissue depots of male *Mmp14*$^{-/-}$ mice (Chun et al., 2006), but the role of MMP14 in the mammary gland stromal fat pad has not been previously appreciated.

Recent studies have emphasized the ability of secreted as well as membrane-anchored MMPs to cleave hundreds of intracellular, cell surface-associated or extracellular substrates (Barbolina and Stack, 2008; Fahlman et al., 2014; Fu et al., 2013; Itoh, 2015; Koziol et al., 2012; Rowe and Weiss, 2009). Given these results, it is surprising, if not perplexing, that global targeting of *Mmp14* or *Mmp15* – as well as *Mmp2* and *Mmp3* – did not derail ductal invasion programs or morphogenesis to a more striking degree. Indeed, while MMP14 has been implicated – to varying, but modest degrees – in early lung, kidney and submandibular gland development, these findings do not extend to mammary gland development (Atkinson

et al., 2005; Oblander et al., 2005; Riggins et al., 2010). While results such as ours are often countered by the argument that the mice genome encodes more than 20 *Mmp* family members, virtually all of these genes have now been targeted, and with the exception of *Mmp14*, each knockout gives rise to viable mice with normal lifespans (Bonnans et al., 2014; Holmbeck et al., 1999; Itoh, 2015; Rowe and Weiss, 2009; Zhou et al., 2000). The fact that only *Mmp14* targeting causes a dramatic increase in the morbidity and mortality of knockout mice (Holmbeck et al., 1999; Zhou et al., 2000), and that dual targeting of *Mmp14* and *Mmp15* results in an embryonic lethal phenotype (Szabova et al., 2010), have, predictably, catalyzed increased efforts to identify the key functions of these proteinases. Clearly, MMP14 and MMP15 *do* exert complex effects on mammary gland development, but the observed changes in function are, for the most part, novel and unanticipated from the perspective of current paradigms.

MATERIALS AND METHODS

Mouse strains

Mmp14$^{lacZ/+}$ mice (Yana et al., 2007) were bred onto a C57Bl/6J background (Jackson Laboratory, 000664). To generate *Mmp15*$^{lacZ/+}$ mice, C57Bl/6J *Mmp15*$^{lacZ/+}$ ES cells clones from the UC Davis KOMP Repository (KOMP) [MGI allele: *Mmp15tm1a* (KOMP) wtsi, clone: EPD0097_3_B09] were introduced into albino C57Bl/6J host blastocysts. The resulting chimeras were mated with C57Bl/6J mice to test for germline transmission. *Mmp15*$^{lacZ/+}$ mice were bred and maintained on a C57Bl/6J background. The *Mmp14*$^{+/-}$ mice (Swiss Black background) were obtained from the National Institutes of Health (Holmbeck et al., 1999) and maintained on an outbred Swiss Black background (Charles River, NIHBL(S)). *Mmp3*$^{-/-}$ mice (C57Bl/6J background) and *Mmp2*$^{-/-}$ mice (Swiss Black background) were genotyped as described (Itoh et al., 1997). To generate *Mmp15* global knockout (*Mmp15*$^{-/-}$) mice, 129/SVJ ES cells were electroporated with a targeting vector for *Mmp15* containing a neomycin selection cassette flanked by FRT sites wherein exons 4 and 5 of the catalytic domain were floxed by loxP sites (Fig. S2A). Following neomycin selection, ES cell recombinants were injected into gestation day E3.5 C57Bl/6J blastocysts that were subsequently injected into the uteri of pseudo-pregnant FVB mice. Male chimeras were mated to C57Bl/6J females, and heterozygous agouti offspring carrying the *Mmp15*^{flox} allele were mated to C57Bl/6J FlpE mice to remove the neomycin selection cassette. The resultant *Mmp15*$^{fl/fl}$ mice were crossed to C57Bl/6J EIIA-Cre mice for germline deletion of *Mmp15* and *Mmp15*$^{+/-}$ mice were backcrossed with C57Bl/6J mice (n>10 generations). All mouse work was performed with the approval of the Institutional Animal Care and Use Committee of the University of Michigan.

Mammary organoid isolation and culture

Organoids were prepared from inguinal mammary glands of P10 mice as described (Fata et al., 2007). Mammary epithelial organoids were then embedded in 2.2 mg/ml acid-extracted rat-tail type I collagen (Sabeh et al., 2009) for 3-D culture in 24-well plates with DMEM/F12 media containing 0.1 mM nonessential amino acids (GIBCO), 0.3 mg/ml L-glutamine, 1X ITS (Sigma, 13146), 10 µg/ml insulin (GIBCO, 12585-014), penicillin and streptomycin, with 50 ng/ml FGF-2 (Simian et al., 2001). Media was changed every 2-3 d for 5-8 d culture periods.

Mammary gland whole mount preparation, imaging and morphometric analysis

Inguinal mammary glands were harvested, mounted on glass slides, stained with Carmine Alum, and processed as described (Lu et al., 2008). Whole mounts were imaged (Leica MZFLIII dissecting microscope) with Adobe Photoshop and ImageJ used to process images (Lu et al., 2008). The length of ductal penetration was quantified as the average distance of straight lines from the nipple to the terminal ends of the four longest mammary epithelial ducts

(Wiseman et al, 2003). The epithelial surface area was quantified as the region occupied by mammary epithelial ducts from the primary stalk to all terminal ends of the branching network. Total branch point number was quantified as the total number of primary, secondary and tertiary branches from the primary stalk of each ductal network.

RNA extraction from intact mammary gland tissue and gene expression analysis

Inguinal mammary gland tissue was flash frozen in liquid nitrogen, homogenized in 1 mL TRIzol (Ambion, Life Technologies). Total RNA was extracted and purified using QIAGEN RNeasy Mini-kit columns (QIAGEN, 74104). RNA quality was confirmed using an Agilent 2100 Bioanalyzer and samples were profiled on Affymetrix Mouse MG–430 PM expression array strips. Expression values for each probe set were calculated using a robust multi-array average (RMA) (Irizarry et al., 2003) and filtered for genes with a greater than 2-fold change. The Affymetrix microarray data were deposited in NCBI's Gene Expression Omnibus (GEO) database (Edgar et al., 2002) and are available through GEO Series accession number GSE77679 (http://www.ncbi.nlm.nih.gov/geo/query/acc.cgi?acc=GSE77679). Complementary cDNA was prepared with the Invitrogen SuperScript II First-Strand Synthesis System (11904-018). Quantitative reverse-transcription PCR was performed with SYBR Green (Applied Biosystems) using *Arbp*/*Rplp0* for reference gene expression. Data reported as the mean expression levels with error bars representing the standard error (SEM). P values were calculated with an unpaired t-test with two tails.

Primers

QPCR primers are provided in Table S1. Genotyping primers are provided in Table S2.

LacZ staining

Inguinal *Mmp14*^{lacZ} mammary glands were fixed at 4ºC in PBS containing 2% paraformaldehyde and 0.2% glutaraldehyde. *Mmp15*^{lacZ} glands were alternatively fixed in 4% paraformaldehyde. Tissues were either transferred to 30% sucrose/PBS (w/v) for frozen sections, or incubated for 18-24 h in PBS containing 4 mM potassium hexacyanoferrate (III), 4 mM potassium hexacyanoferrate (II) trihydrate, 2 mM $MgCl_2$, 0.2% NP-40, 0.1% sodium deoxycholic acid and 1 mg/ml Xgal. Stained tissues and whole mounts were post-fixed with 10% formalin-phosphate.

Immunofluorescence, immunohistochemistry and morphometric analysis.

Mammary gland tissue was fixed in 10% formalin-phosphate at 4º C overnight and either dehydrated in an ethanol/paraffin series for paraffin embedding or transferred to 30% (w/v) sucrose/PBS for embedding in OCT. Sections were permeabilized with 0.3-0.5% Triton X-

100/ PBS, and blocked for 2 h prior to primary antibody addition. Samples were incubated overnight at 4°C with antibodies directed against [ZO-1 (Invitrogen, 617300, 2.5 µg/ml), E-cadherin (BD Transduction Laboratories, 610181, 1/400), Cytokeratin-14 (Covance, PRB-155P, Clone AF64, 1/400), Cytokeratin-18 (Abcam, ab668, 1/150), α-smooth muscle actin (Abcam, ab5694, 1/400), or UCP1 (Alpha Diagnostic International, UCP11-A, 200 ng/ml)]. For ECM staining, frozen sections were incubated in blocking buffer (10% FBS/1% BSA/PBS) and incubated with primary antibodies directed against Type IV collagen antibody (Millipore, AB-769, 1/40) (Nguyen-Ngoc et al., 2012), Laminin antibody (Sigma-Aldrich, L9393, 1/250), or Type I collagen (Abcam, ab34710, 1/250) overnight at 4°C. Following primary antibody incubations, sections were incubated with Alexa-488 or Alexa-594-conjugated secondary antibodies (Invitrogen Molecular Probes). Nuclear counter-staining was carried out with either Toto3 (1:200, Invitrogen Molecular Probes) or 2 µg/ml 4, 6-diamidino-2-phenylindole (DAPI). All fluorescence images were acquired with an Olympus FluoView FV500 laser scanning confocal microscope and analyzed with Adobe Photoshop and ImageJ software. For immunohistochemistry, endogenous peroxidase activity was blocked with 3% H_2O_2 and tissues sections developed with the Vectastain ABC kit (Vector Laboratories, PK-6100) and DAB kit (Vector Laboratories, SK-4100). ImageJ was used to measure the diameter of n>20 adipocytes per 40X field of H&E-stained paraffin cross-sections.

Tissue preparation for TEM

Samples were fixed (1% glutaraldehyde/ 1% tannic acid/ 0.1 M Sorensen's buffer, pH 7.2) and post-fixed with 1% osmium tetroxide as described (Abrahamson and Perry, 1986) prior to embedding in EMbed 812 epoxy resin (Electron Microscopy Sciences). Thin sections (70 nm) were post-stained with uranyl acetate and Reynolds Lead Citrate, and imaged with a JE0L JEM-1400 Plus electron microscope at 80 kV. Images were recorded digitally using a Hamamatsu ORCA-HR digital camera system, operated using AMT software (Advanced Microscopy Techniques Corp., Danvers, MA). ImageJ was used to quantify average number of microvilli per µm from n > 5 fields per sample and n = 3 per genotype; and to quantify the surface area of individual mitochondria in n>10 fields per sample and n=2 per genotype. Results are expressed as mean ± SEM.

Acknowledgements

We thank Alan Saltiel (UC San Diego) and David Ginsburg (University of Michigan) for helpful discussions. We acknowledge Dorothy Sorenson (University of Michigan) for assistance with TEM and Craig Johnson (University of Michigan) for assistance with microarray analysis.

Competing interests statement

The authors declare no competing financial interests.

Author Contributions

TYF and SJW designed research; TYF performed experiments; TYF, RGR and TLS contributed new reagents/analytical tools; TYF and SJW analyzed the data and wrote paper.

Funding

This work was supported by a grant from the Breast Cancer Research Foundation (SJW) and from the NIH CA071699 (SJW).

REFERENCES

Abraham, R., J. Schafer, M. Rothe, J. Bange, P. Knyazev and A. Ullrich (2005). Identification of MMP-15 as an anti-apoptotic factor in cancer cells. *J Biol Chem* **280**, 34123-34132.

Abrahamson, D. R. and E. W. Perry (1986). Evidence for splicing new basement membrane into old during glomerular development in newborn rat kidneys. *J Cell Biol* **103**, 2489-2498.

Ager, E. I., S. V. Kozin, N. D. Kirkpatrick, G. Seano, D. P. Kodack, V. Askoxylakis, Y. Huang, S. Goel, M. Snuderl, A. Muzikansky, et al. (2015). Blockade of MMP14 activity in murine breast carcinomas: implications for macrophages, vessels, and radiotherapy. *J Natl Cancer Inst* **107**.

Ahmad, M., S. Attoub, M. N. Singh, F. L. Martin and O. M. El-Agnaf (2007). Gamma-synuclein and the progression of cancer. *FASEB J* **21**, 3419-3430.

Alcaraz, J., H. Mori, C. M. Ghajar, D. Brownfield, R. Galgoczy and M. J. Bissell (2011). Collective epithelial cell invasion overcomes mechanical barriers of collagenous extracellular matrix by a narrow tube-like geometry and MMP14-dependent local softening. *Integr Biol (Camb)* **3**, 1153-1166.

Arimoto, K., C. Burkart, M. Yan, D. Ran, S. Weng and D. E. Zhang (2014). Plakophilin-2 promotes tumor development by enhancing ligand-dependent and -independent epidermal growth factor receptor dimerization and activation. *Mol Cell Biol* **34**, 3843-3854.

Atkinson, J. J., K. Holmbeck, S. Yamada, H. Birkedal-Hansen, W. C. Parks and R. M. Senior (2005). Membrane-type 1 matrix metalloproteinase is required for normal alveolar development. *Dev Dyn* **232**, 1079-1090.

Barbolina, M. V. and M. S. Stack (2008). Membrane type 1-matrix metalloproteinase: substrate diversity in pericellular proteolysis. *Semin Cell Dev Biol* **19**, 24-33.

Bonnans, C., J. Chou and Z. Werb (2014). Remodelling the extracellular matrix in development and disease. *Nat Rev Mol Cell Biol* **15**, 786-801.

Chun, T. H., K. B. Hotary, F. Sabeh, A. R. Saltiel, E. D. Allen and S. J. Weiss (2006). A pericellular collagenase directs the 3-dimensional development of white adipose tissue. *Cell* **125**, 577-591.

Chun, T. H., F. Sabeh, I. Ota, H. Murphy, K. T. McDonagh, K. Holmbeck, H. Birkedal-Hansen, E. D. Allen and S. J. Weiss (2004). MT1-MMP-dependent neovessel formation within the confines of the three-dimensional extracellular matrix. *J Cell Biol* **167**, 757-767.

Cohen, P., J. D. Levy, Y. Zhang, A. Frontini, D. P. Kolodin, K. J. Svensson, J. C. Lo, X. Zeng, L. Ye, M. J. Khandekar, et al. (2014). Ablation of PRDM16 and beige adipose causes metabolic dysfunction and a subcutaneous to visceral fat switch. *Cell* **156**, 304-316.

Correia, A. L., H. Mori, E. I. Chen, F. C. Schmitt and M. J. Bissell (2013). The hemopexin domain of MMP3 is responsible for mammary epithelial invasion and morphogenesis through extracellular interaction with HSP90beta. *Genes Dev* **27**, 805-817.

Edgar, R., M. Domrachev and A. E. Lash (2002). Gene Expression Omnibus: NCBI gene expression and hybridization array data repository. *Nucleic Acids Res* **30**, 207-210.

Ewald, A. J., A. Brenot, M. Duong, B. S. Chan and Z. Werb (2008). Collective epithelial migration and cell rearrangements drive mammary branching morphogenesis. *Dev Cell* **14**, 570-581.

Ewald, A. J., R. J. Huebner, H. Palsdottir, J. K. Lee, M. J. Perez, D. M. Jorgens, A. N. Tauscher, K. J. Cheung, Z. Werb and M. Auer (2012). Mammary collective cell migration involves transient loss of epithelial features and individual cell migration within the epithelium. *J Cell Sci* **125**, 2638-2654.

Fahlman, R. P., W. Chen and C. M. Overall (2014). Absolute proteomic quantification of the activity state of proteases and proteolytic cleavages using proteolytic signature peptides and isobaric tags. *J Proteomics* **100**, 79-91.

Fata, J. E., H. Mori, A. J. Ewald, H. Zhang, E. Yao, Z. Werb and M. J. Bissell (2007). The MAPK(ERK-1,2) pathway integrates distinct and antagonistic signals from TGFalpha and FGF7 in morphogenesis of mouse mammary epithelium. *Dev Biol* **306**, 193-207.

Fu, H. L., A. Sohail, R. R. Valiathan, B. D. Wasinski, M. Kumarasiri, K. V. Mahasenan, M. M. Bernardo, D. Tokmina-Roszyk, G. B. Fields, S. Mobashery, et al. (2013). Shedding of discoidin domain receptor 1 by membrane-type matrix metalloproteinases. *J Biol Chem* **288**, 12114-12129.

Gouon-Evans, V. and J. W. Pollard (2002). Unexpected deposition of brown fat in mammary gland during postnatal development. *Mol Endocrinol* **16**, 2618-2627.

Gutierrez-Fernandez, A., C. Soria-Valles, F. G. Osorio, J. Gutierrez-Abril, C. Garabaya, A. Aguirre, A. Fueyo, M. S. Fernandez-Garcia, X. S. Puente and C. Lopez-Otin (2015). Loss of MT1-MMP causes cell senescence and nuclear defects which can be reversed by retinoic acid. *EMBO J* **34**, 1875-1888.

Harms, M. J., J. Ishibashi, W. Wang, H. W. Lim, S. Goyama, T. Sato, M. Kurokawa, K. J. Won and P. Seale (2014). Prdm16 is required for the maintenance of brown adipocyte identity and function in adult mice. *Cell Metab* **19**, 593-604.

Harunaga, J. S., A. D. Doyle and K. M. Yamada (2014). Local and global dynamics of the basement membrane during branching morphogenesis require protease activity and actomyosin contractility. *Dev Biol* **394**, 197-205.

Haslam, S. Z., A. Drolet, K. Smith, M. Tan and M. Aupperlee (2008). Progestin-regulated luminal cell and myoepithelial cell-specific responses in mammary organoid culture. *Endocrinology* **149**, 2098-2107.

Hogg, N. A., C. J. Harrison and C. Tickle (1983). Lumen formation in the developing mouse mammary gland. *J Embryol Exp Morphol* **73**, 39-57.

Holmbeck, K., P. Bianco, J. Caterina, S. Yamada, M. Kromer, S. A. Kuznetsov, M. Mankani, P. G. Robey, A. R. Poole, I. Pidoux, et al. (1999). MT1-MMP-deficient mice develop dwarfism, osteopenia, arthritis, and connective tissue disease due to inadequate collagen turnover. *Cell* **99**, 81-92.

Hotary, K., E. Allen, A. Punturieri, I. Yana and S. J. Weiss (2000). Regulation of cell invasion and morphogenesis in a three-dimensional type I collagen matrix by membrane-type matrix metalloproteinases 1, 2, and 3. *J Cell Biol* **149**, 1309-1323.

Hovey, R. C. and L. Aimo (2010). Diverse and active roles for adipocytes during mammary gland growth and function. *J Mammary Gland Biol Neoplasia* **15**, 279-290.

Huebner, R. J. and A. J. Ewald (2014). Cellular foundations of mammary tubulogenesis. *Semin Cell Dev Biol* **31**, 124-131.

Inman, J. L., C. Robertson, J. D. Mott and M. J. Bissell (2015). Mammary gland development: cell fate specification, stem cells and the microenvironment. *Development* **142**, 1028-1042.

Irizarry, R. A., B. Hobbs, F. Collin, Y. D. Beazer-Barclay, K. J. Antonellis, U. Scherf and T. P. Speed (2003). Exploration, normalization, and summaries of high density oligonucleotide array probe level data. *Biostatistics* **4**, 249-264.

Itoh, T., T. Ikeda, H. Gomi, S. Nakao, T. Suzuki and S. Itohara (1997). Unaltered secretion of beta-amyloid precursor protein in gelatinase A (matrix metalloproteinase 2)-deficient mice. *J Biol Chem* **272**, 22389-22392.

Itoh, Y. (2015). Membrane-type matrix metalloproteinases: Their functions and regulation. *Matrix Biol* **44-46**, 207-223.

Kajita, M., Y. Itoh, T. Chiba, H. Mori, A. Okada, H. Kinoh and M. Seiki (2001). Membrane-type 1 matrix metalloproteinase cleaves CD44 and promotes cell migration. *J Cell Biol* **153**, 893-904.

Kessenbrock, K., G. J. Dijkgraaf, D. A. Lawson, L. E. Littlepage, P. Shahi, U. Pieper and Z. Werb (2013). A role for matrix metalloproteinases in regulating mammary stem cell function via the Wnt signaling pathway. *Cell Stem Cell* **13**, 300-313.

Khabibullin, D., D. A. Medvetz, M. Pinilla, V. Hariharan, C. Li, A. Hergrueter, M. Laucho Contreras, E. Zhang, A. Parkhitko, J. J. Yu, et al. (2014). Folliculin regulates cell-cell adhesion, AMPK, and mTORC1 in a cell-type-specific manner in lung-derived cells. *Physiol Rep* **2**, e12107.

Koshikawa, N., G. Giannelli, V. Cirulli, K. Miyazaki and V. Quaranta (2000). Role of cell surface metalloprotease MT1-MMP in epithelial cell migration over laminin-5. *J Cell Biol* **148**, 615-624.

Koziol, A., P. Gonzalo, A. Mota, A. Pollan, C. Lorenzo, N. Colome, D. Montaner, J. Dopazo, J. Arribas, F. Canals, et al. (2012). The protease MT1-MMP drives a combinatorial proteolytic program in activated endothelial cells. *FASEB J* **26**, 4481-4494.

Liesa, M. and O. S. Shirihai (2013). Mitochondrial dynamics in the regulation of nutrient utilization and energy expenditure. *Cell Metab* **17**, 491-506.

Lo, A. T., H. Mori, J. Mott and M. J. Bissell (2012). Constructing three-dimensional models to study mammary gland branching morphogenesis and functional differentiation. *J Mammary Gland Biol Neoplasia* **17**, 103-110.

Lochter, A., S. Galosy, J. Muschler, N. Freedman, Z. Werb and M. J. Bissell (1997). Matrix metalloproteinase stromelysin-1 triggers a cascade of molecular alterations that leads to stable epithelial-to-mesenchymal conversion and a premalignant phenotype in mammary epithelial cells. *J Cell Biol* **139**, 1861-1872.

Londhe, V. A., T. M. Maisonet, B. Lopez, B. C. Shin, J. Huynh and S. U. Devaskar (2013). Retinoic acid rescues alveolar hypoplasia in the calorie-restricted developing rat lung. *Am J Respir Cell Mol Biol* **48**, 179-187.

Loo, C. S., C. W. Chen, P. J. Wang, P. Y. Chen, S. Y. Lin, K. H. Khoo, R. A. Fenton, M. A. Knepper and M. J. Yu (2013). Quantitative apical membrane proteomics reveals vasopressin-induced actin dynamics in collecting duct cells. *Proc Natl Acad Sci U S A* **110**, 17119-17124.

Lu, P., A. J. Ewald, G. R. Martin and Z. Werb (2008). Genetic mosaic analysis reveals FGF receptor 2 function in terminal end buds during mammary gland branching morphogenesis. *Dev Biol* **321**, 77-87.

Macias, H. and L. Hinck (2012). Mammary gland development. *Wiley Interdiscip Rev Dev Biol* **1**, 533-557.

Marsili, A., C. Aguayo-Mazzucato, T. Chen, A. Kumar, M. Chung, E. P. Lunsford, J. W. Harney, T. Van-Tran, E. Gianetti, W. Ramadan, et al. (2011). Mice with a targeted deletion of the type 2 deiodinase are insulin resistant and susceptible to diet induced obesity. *PLoS One* **6**, e20832.

Master, S. R., J. L. Hartman, C. M. D'Cruz, S. E. Moody, E. A. Keiper, S. I. Ha, J. D. Cox, G. K. Belka and L. A. Chodosh (2002). Functional microarray analysis of mammary organogenesis reveals a developmental role in adaptive thermogenesis. *Mol Endocrinol* **16**, 1185-1203.

Mori, H., N. Gjorevski, J. L. Inman, M. J. Bissell and C. M. Nelson (2009). Self-organization of engineered epithelial tubules by differential cellular motility. *Proc Natl Acad Sci U S A* **106**, 14890-14895.

Mori, H., A. T. Lo, J. L. Inman, J. Alcaraz, C. M. Ghajar, J. D. Mott, C. M. Nelson, C. S. Chen, H. Zhang, J. L. Bascom, et al. (2013). Transmembrane/cytoplasmic, rather than catalytic, domains of Mmp14 signal to MAPK activation and mammary branching morphogenesis via binding to integrin beta1. *Development* **140**, 343-352.

Nelson, D. A. and M. Larsen (2015). Heterotypic control of basement membrane dynamics during branching morphogenesis. *Dev Biol* **401**, 103-109.

Nguyen-Ngoc, K. V., K. J. Cheung, A. Brenot, E. R. Shamir, R. S. Gray, W. C. Hines, P. Yaswen, Z. Werb and A. J. Ewald (2012). ECM microenvironment regulates collective migration and local dissemination in normal and malignant mammary epithelium. *Proc Natl Acad Sci U S A* **109**, E2595-2604.

Oblander, S. A., Z. Zhou, B. G. Galvez, B. Starcher, J. M. Shannon, M. Durbeej, A. G. Arroyo, K. Tryggvason and S. S. Apte (2005). Distinctive functions of membrane type 1 matrix-metalloprotease (MT1-MMP or MMP-14) in lung and submandibular gland development are independent of its role in pro-MMP-2 activation. *Dev Biol* **277**, 255-269.

Oh, J., R. Takahashi, E. Adachi, S. Kondo, S. Kuratomi, A. Noma, D. B. Alexander, H. Motoda, A. Okada, M. Seiki, et al. (2004). Mutations in two matrix metalloproteinase genes, MMP-2 and MT1-MMP, are synthetic lethal in mice. *Oncogene* **23**, 5041-5048.

Ota, I., X. Y. Li, Y. Hu and S. J. Weiss (2009). Induction of a MT1-MMP and MT2-MMP-dependent basement membrane transmigration program in cancer cells by Snail1. *Proc Natl Acad Sci U S A* **106**, 20318-20323.

Rebustini, I. T., C. Myers, K. S. Lassiter, A. Surmak, L. Szabova, K. Holmbeck, V. Pedchenko, B. G. Hudson and M. P. Hoffman (2009). MT2-MMP-dependent release of collagen IV NC1 domains regulates submandibular gland branching morphogenesis. *Dev Cell* **17**, 482-493.

Riggins, K. S., G. Mernaugh, Y. Su, V. Quaranta, N. Koshikawa, M. Seiki, A. Pozzi and R. Zent (2010). MT1-MMP-mediated basement membrane remodeling modulates renal development. *Exp Cell Res* **316**, 2993-3005.

Rowe, R. G. and S. J. Weiss (2008). Breaching the basement membrane: who, when and how? *Trends Cell Biol* **18**, 560-574.

Rowe, R. G. and S. J. Weiss (2009). Navigating ECM barriers at the invasive front: the cancer cell-stroma interface. *Annu Rev Cell Dev Biol* **25**, 567-595.

Sabeh, F., R. Shimizu-Hirota and S. J. Weiss (2009). Protease-dependent versus -independent cancer cell invasion programs: three-dimensional amoeboid movement revisited. *J Cell Biol* **185**, 11-19.

Sakamoto, T., J. S. Weng, T. Hara, S. Yoshino, H. Kozuka-Hata, M. Oyama and M. Seiki (2014). Hypoxia-inducible factor 1 regulation through cross talk between mTOR and MT1-MMP. *Mol Cell Biol* **34**, 30-42.

Shimizu-Hirota, R., W. Xiong, B. T. Baxter, S. L. Kunkel, I. Maillard, X. W. Chen, F. Sabeh, R. Liu, X. Y. Li and S. J. Weiss (2012). MT1-MMP regulates the PI3Kdelta.Mi-2/NuRD-dependent control of macrophage immune function. *Genes Dev* **26**, 395-413.

Simian, M., Y. Hirai, M. Navre, Z. Werb, A. Lochter and M. J. Bissell (2001). The interplay of matrix metalloproteinases, morphogens and growth factors is necessary for branching of mammary epithelial cells. *Development* **128**, 3117-3131.

Stresing, V., E. Baltziskueta, N. Rubio, J. Blanco, M. C. Arriba, J. Valls, M. Janier, P. Clezardin, R. Sanz-Pamplona, C. Nieva, et al. (2013). Peroxiredoxin 2 specifically regulates

the oxidative and metabolic stress response of human metastatic breast cancer cells in lungs. *Oncogene* **32**, 724-735.

Sun, P., Y. Yuan, A. Li, B. Li and X. Dai (2010). Cytokeratin expression during mouse embryonic and early postnatal mammary gland development. *Histochem Cell Biol* **133**, 213-221.

Szabova, L., M. Y. Son, J. Shi, M. Sramko, S. S. Yamada, W. D. Swaim, P. Zerfas, S. Kahan and K. Holmbeck (2010). Membrane-type MMPs are indispensable for placental labyrinth formation and development. *Blood* **116**, 5752-5761.

Szabova, L., S. S. Yamada, H. Birkedal-Hansen and K. Holmbeck (2005). Expression pattern of four membrane-type matrix metalloproteinases in the normal and diseased mouse mammary gland. *J Cell Physiol* **205**, 123-132.

Tan, J., E. Buache, F. Alpy, E. Daguenet, C. L. Tomasetto, G. S. Ren and M. C. Rio (2014). Stromal matrix metalloproteinase-11 is involved in the mammary gland postnatal development. *Oncogene* **33**, 4050-4059.

Tang, Y., R. G. Rowe, E. L. Botvinick, A. Kurup, A. J. Putnam, M. Seiki, V. M. Weaver, E. T. Keller, S. Goldstein, J. Dai, et al. (2013). MT1-MMP-dependent control of skeletal stem cell commitment via a beta1-integrin/YAP/TAZ signaling axis. *Dev Cell* **25**, 402-416.

Taylor, S. H., C. Y. Yeung, N. S. Kalson, Y. Lu, P. Zigrino, T. Starborg, S. Warwood, D. F. Holmes, E. G. Canty-Laird, C. Mauch, et al. (2015). Matrix metalloproteinase 14 is required for fibrous tissue expansion. *Elife* **4**, e09345.

Ucar, A., V. Vafaizadeh, H. Jarry, J. Fiedler, P. A. Klemmt, T. Thum, B. Groner and K. Chowdhury (2010). miR-212 and miR-132 are required for epithelial stromal interactions necessary for mouse mammary gland development. *Nat Genet* **42**, 1101-1108.

Varner, V. D. and C. M. Nelson (2014). Cellular and physical mechanisms of branching morphogenesis. *Development* **141**, 2750-2759.

Vergnes, L., R. Chin, S. G. Young and K. Reue (2011). Heart-type fatty acid-binding protein is essential for efficient brown adipose tissue fatty acid oxidation and cold tolerance. *J Biol Chem* **286**, 380-390.

Wang, Q. A., C. Tao, L. Jiang, M. Shao, R. Ye, Y. Zhu, R. Gordillo, A. Ali, Y. Lian, W. L. Holland, et al. (2015). Distinct regulatory mechanisms governing embryonic versus adult adipocyte maturation. *Nat Cell Biol* **17**, 1099-1111.

Watson, C. J. and W. T. Khaled (2008). Mammary development in the embryo and adult: a journey of morphogenesis and commitment. *Development* **135**, 995-1003.

Weaver, S. A., B. Wolters, N. Ito, A. M. Woskowicz, K. Kaneko, Y. Shitomi, M. Seiki and Y. Itoh (2014). Basal localization of MT1-MMP is essential for epithelial cell morphogenesis in 3D collagen matrix. *J Cell Sci* **127**, 1203-1213.

Williams, J. M. and C. W. Daniel (1983). Mammary ductal elongation: differentiation of myoepithelium and basal lamina during branching morphogenesis. *Dev Biol* **97**, 274-290.

Wiseman, B. S., M. D. Sternlicht, L. R. Lund, C. M. Alexander, J. Mott, M. J. Bissell, P. Soloway, S. Itohara and Z. Werb (2003). Site-specific inductive and inhibitory activities of MMP-2 and MMP-3 orchestrate mammary gland branching morphogenesis. *J Cell Biol* **162**, 1123-1133.

Witty, J. P., J. H. Wright and L. M. Matrisian (1995). Matrix metalloproteinases are expressed during ductal and alveolar mammary morphogenesis, and misregulation of stromelysin-1 in transgenic mice induces unscheduled alveolar development. *Mol Biol Cell* **6**, 1287-1303.

Wu, J., P. Cohen and B. M. Spiegelman (2013). Adaptive thermogenesis in adipocytes: is beige the new brown? *Genes Dev* **27**, 234-250.

Yana, I., H. Sagara, S. Takaki, K. Takatsu, K. Nakamura, K. Nakao, M. Katsuki, S. Taniguchi, T. Aoki, H. Sato, et al. (2007). Crosstalk between neovessels and mural cells directs the site-specific expression of MT1-MMP to endothelial tip cells. *J Cell Sci* **120**, 1607-1614.

Zhou, Z., S. S. Apte, R. Soininen, R. Cao, G. Y. Baaklini, R. W. Rauser, J. Wang, Y. Cao and K. Tryggvason (2000). Impaired endochondral ossification and angiogenesis in mice deficient in membrane-type matrix metalloproteinase I. *Proc Natl Acad Sci U S A* **97**, 4052-4057.

Figures

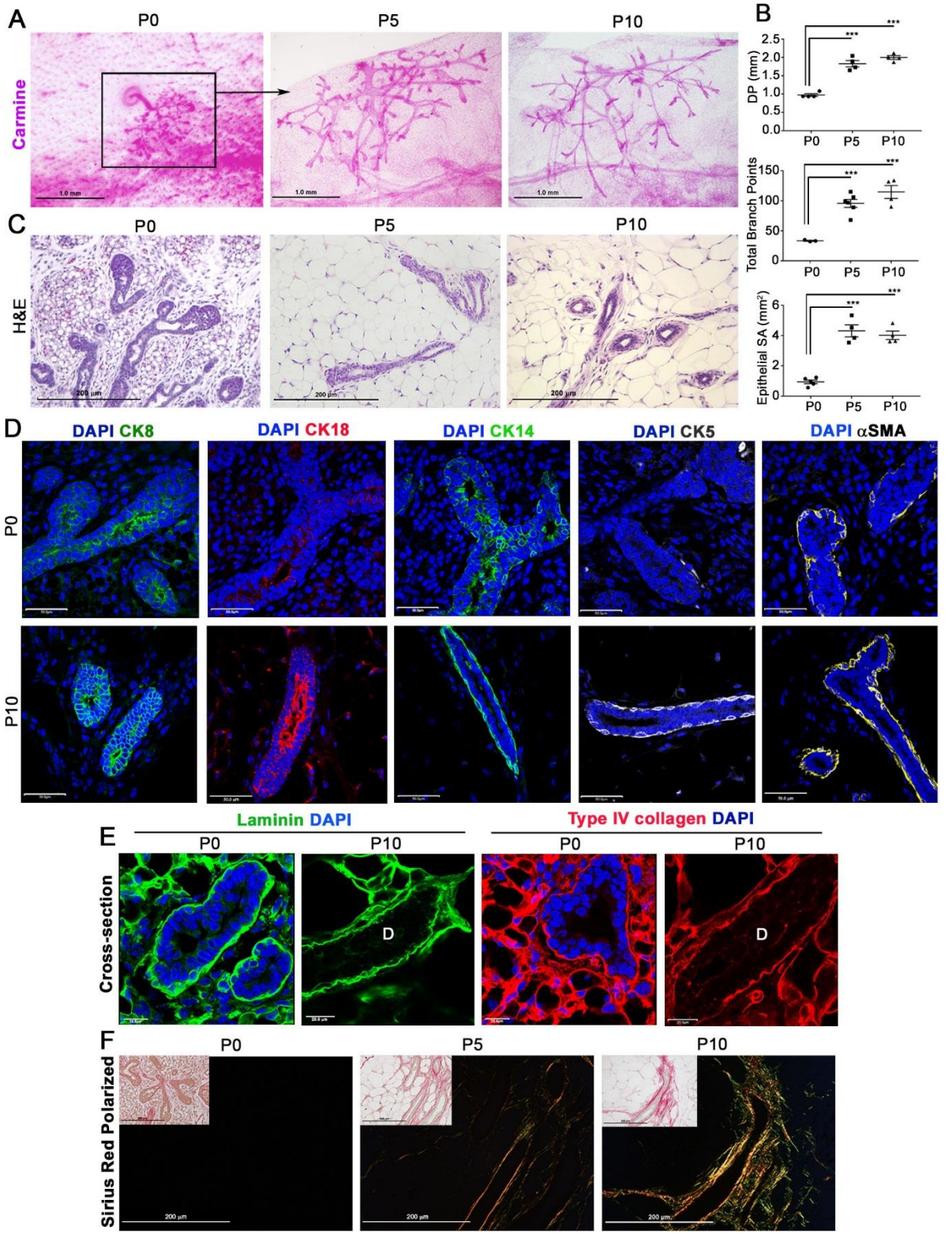

Figure 1. Early postnatal mammary gland morphogenesis program. (A) Carmine-stained whole mounts of mammary glands isolated from female mice at P0, P5 and P10 (scale bars = 1.0 mm). (B) Quantification of mammary gland ductal penetration (DP) (mm), total branch point number and epithelial surface area (mm^2) at P0, P5 and P10 with mean ± SEM (n>3). ***p<0.001, as calculated with an unpaired t-test. (C) H&E staining of cross-sections of mammary glands at P0, P5 and P10 (scale bar = 200 μm). (D) Immunofluorescence of cytokeratin-8 (CK8), cytokeratin-18 (CK18), cytokeratin-14 (CK14), cytokeratin-5 (CK5) and α-smooth muscle actin (α-SMA) in P0 versus P10 mammary glands with DAPI-mediated nuclear counter-staining (scale bars = 50.0 μm). (E) Immunofluorescence of laminin and type IV collagen in P0 and P10 mammary glands with DAPI counter-staining (scale bars = 50.0 μm). (E) Polarized light images of Sirius Red staining of P0, P5 and P10 mammary gland cross-sections. Insets show the corresponding bright-field images (scale bars = 200 μm). All images are representative of 3 replicates.

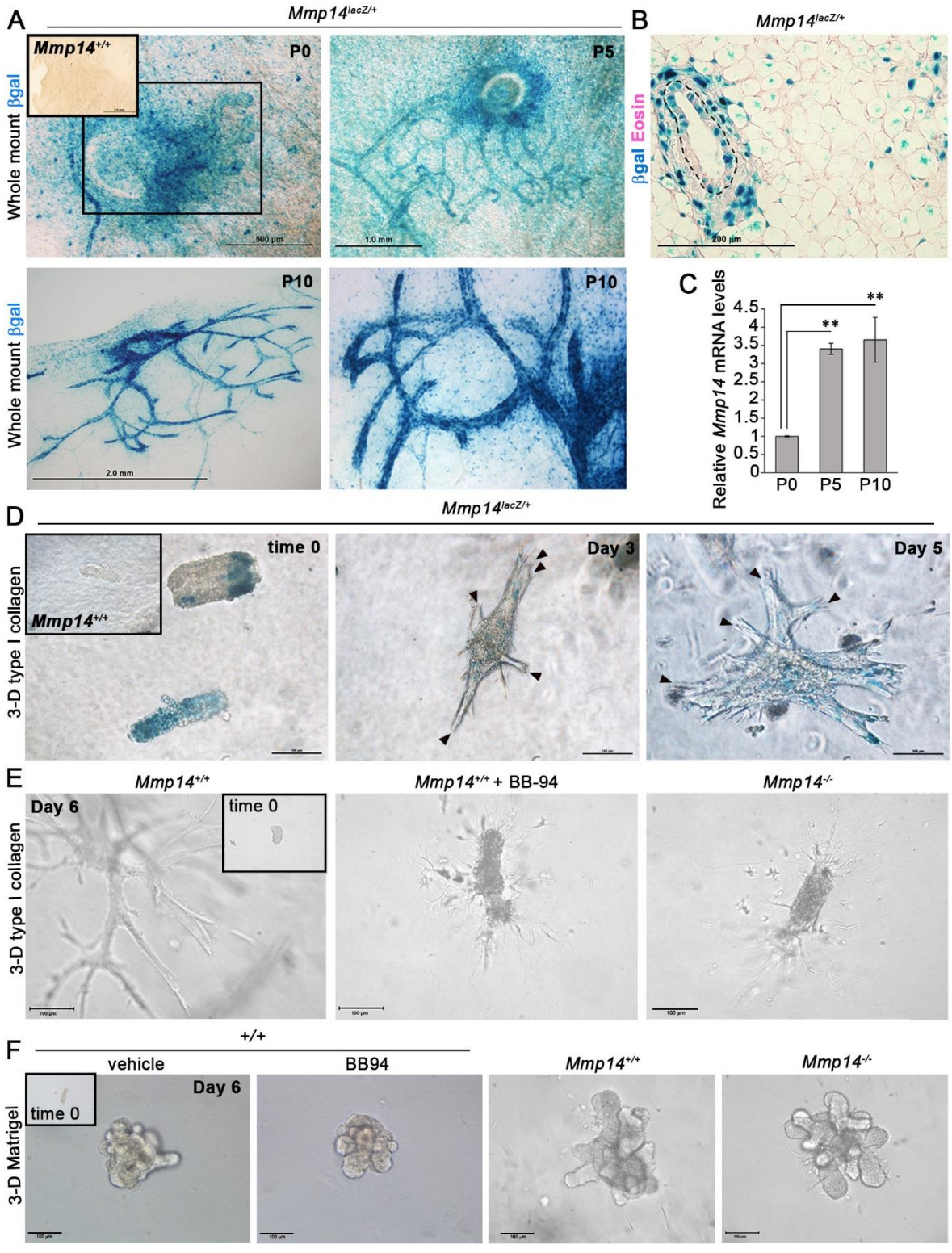

Figure 2. ***In vitro*** **mammary epithelial branching requires MMP14.** (A) LacZ staining of mammary gland whole mounts isolated from *Mmp14*$^{lacZ/+}$ mice at P0, P5, and P10 (scale bars = 500 μm, 1.0 mm, and 2.0 mm, respectively). The inset shows LacZ staining of the wild-type littermate. (B) Paraffin cross-section through P10 *Mmp14*$^{lacZ/+}$ mammary gland with Eosin counterstaining. Images shown in A, B are representative of 3 replicates. (C) qPCR of *Mmp14* at P0, P5 and P10. Results are expressed as mean expression levels ± SEM of P0 (n=4), P5

(n=3) and P10 (n=4) relative to *Arbp*. **p<0.005, as calculated with an unpaired t-test. (D) LacZ staining of *Mmp14*$^{lacZ/+}$ mammary epithelial organoids cultured in 3-D type I collagen with serum-free media containing 50 ng/ml FGF-2 at time 0, day 3 and day 5 (scale bar = 100 μm). The inset shows LacZ staining of wild-type littermate organoids. Arrow heads denote LacZ-negative terminal ends. (E,F) Phase contrast images of *Mmp14*$^{+/+}$ and *Mmp14*$^{-/-}$ mammary epithelial organoids isolated from mice at P10 and embedded within 3-D type I collagen or 3-D Matrigel for 6 days with 50 ng/ml FGF-2 alone, or with FGF-2 in the presence of 5 μm BB-94 (scale bar = 100 μm) . The insets show the mammary epithelial organoids at time 0. Results are representative of 5 experiments performed.

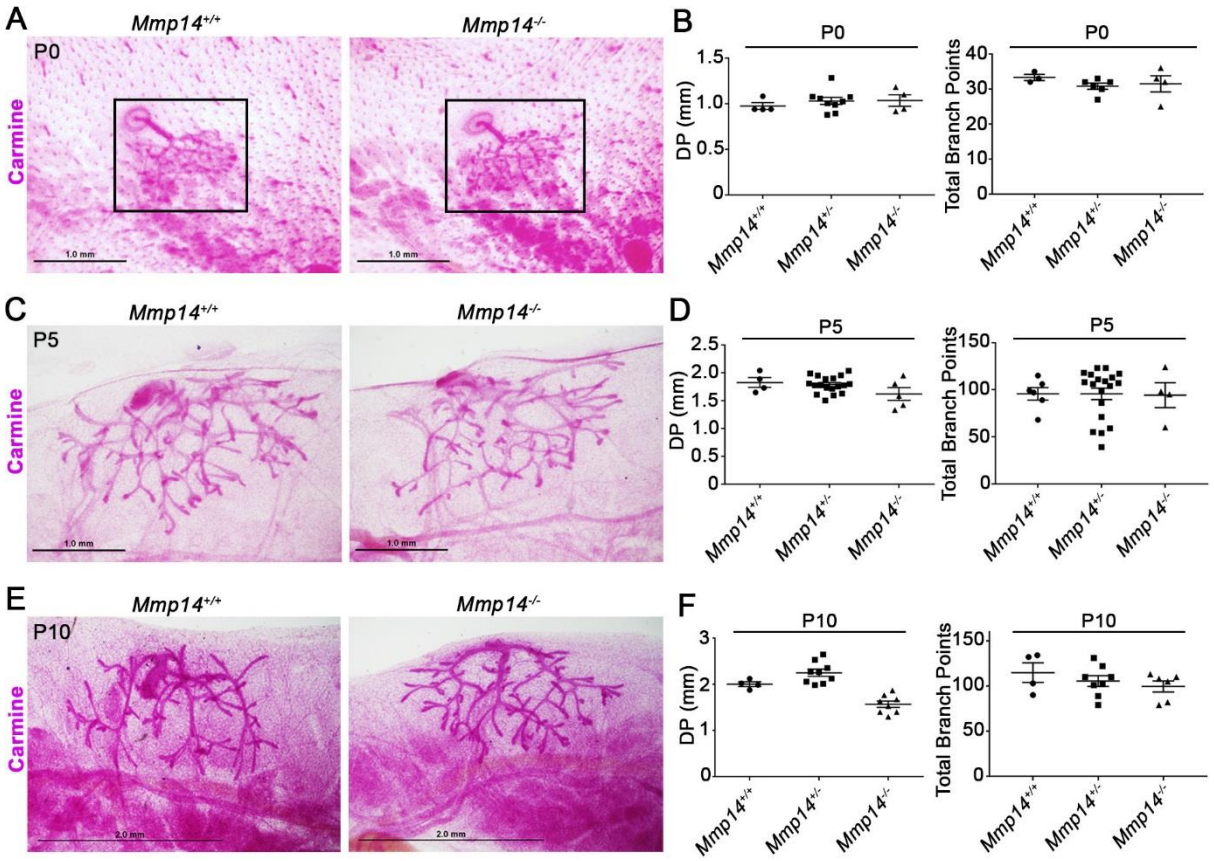

Figure 3. Early mammary gland branching proceeds independently of MMP14. (A,C,E) Carmine-stained whole mounts of mammary glands isolated from representative P0, P5, and P10 *Mmp14*$^{+/+}$ vs. *Mmp14*$^{-/-}$ female mice. (B,D,F). Ductal penetration (DP) (mm) and total branch point quantifications of *Mmp14*$^{+/+}$, *Mmp14*$^{+/-}$ and *Mmp14*$^{-/-}$ mice at P0, P5, and P10. Results are plotted with mean ± SEM in *Mmp14*$^{+/+}$ (n=4 per time-point), *Mmp14*$^{+/-}$ mice at P0 (n=9), P5 (n=18) and P10 (n=9), and *Mmp14*$^{-/-}$ mice at P0 (n=4), P5 (n=5) and P10 (n=8). Scale bars represent 500 μm, 1.0 mm, and 2.0 mm, respectively.

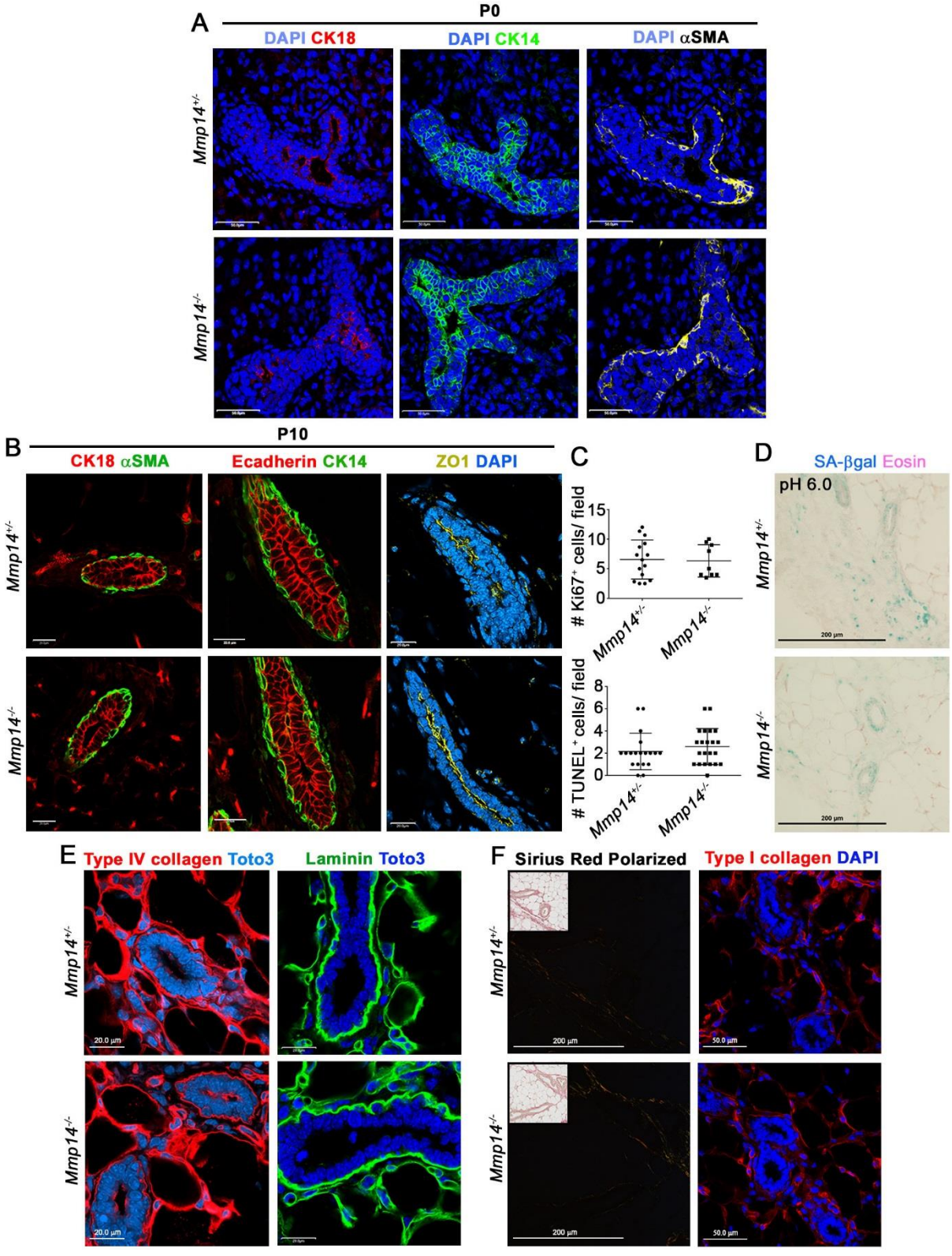

Figure 4. MMP14-independent epithelial cell sorting, proliferation, senescence and ECM organization. (A) Immunofluorescence of cytokeratin-18 (CK18), cytokeratin-14 (CK14) and α-smooth muscle actin (αSMA) in P0 *Mmp14*$^{+/+}$ vs. *Mmp14*$^{-/-}$ mammary glands with DAPI counter-staining (scale bars = 50 µm). (B) Immunofluorescence of CK18 and αSMA (left), E-

cadherin and CK14 (middle), and Zonula occludens (ZO)-1 with DAPI counter-staining (right) in P10 *Mmp14*$^{+/+}$ vs. *Mmp14*$^{-/-}$ mammary glands (scale bars = 50 μm). (C) Quantifications of average number of Ki67-positive cells per field and TUNEL-positive cells per field from immunofluorescence of P5 mammary glands at 60X magnification (n=2 per genotype). Results are plotted with mean values of n>10 fields ± 1 SD. (D) Senescence-associated β-galactosidase (SA-βgal) staining of P5 *Mmp14*$^{+/+}$ vs. *Mmp14*$^{-/-}$ mammary glands under pH 6.0 conditions (n=2 per genotype, scale bar = 200 μm). (E) Immunofluorescence of type IV collagen and laminin in P5 *Mmp14*$^{+/+}$ vs. *Mmp14*$^{-/-}$ mammary glands with Toto3-mediated nuclear counter-staining (scale bar = 50 μm). (F) Polarized light images of Sirius Red staining of P5 *Mmp14*$^{+/+}$ vs. *Mmp14*$^{-/-}$ mammary gland cross-sections . Insets show the corresponding bright-field images (scale bar = 200 μm). Type I collagen immunofluorescence in P5 wild-type versus knockout mammary glands with DAPI counter-staining (scale bar = 50.0 μm). All images are representative of 3 replicates.

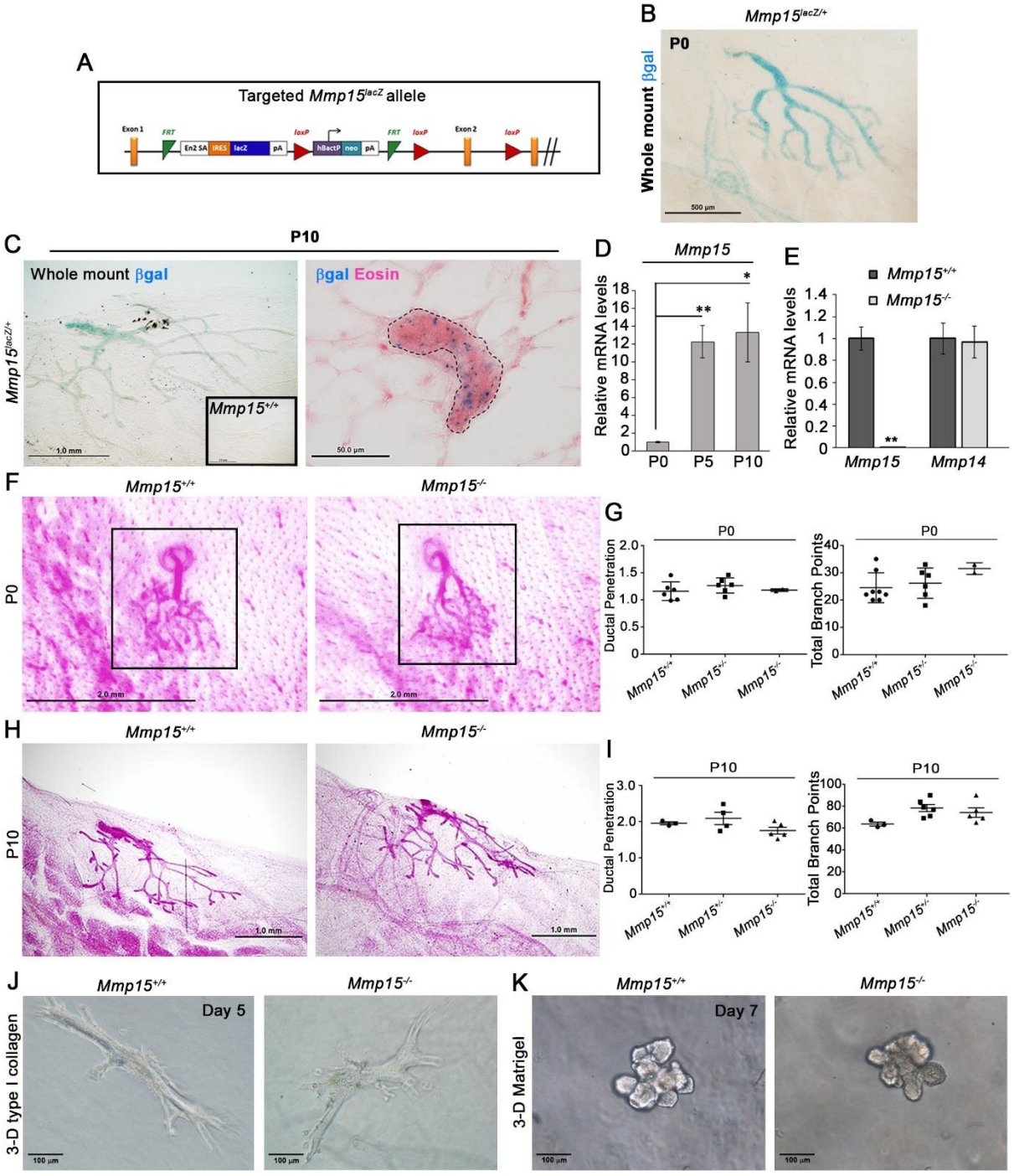

Figure 5. Early mammary epithelial branching is *Mmp15*-independent. (A) Schematic of targeted *Mmp15*^{lacZ} allele. (B) LacZ staining of P0 *Mmp15*$^{lacZ/+}$ mammary gland whole mount. (C) LacZ staining of P10 *Mmp15*$^{lacZ/+}$ whole mount (left panel). Inset shows LacZ staining of wild-type mammary tissue. In the right panel, a P10 *Mmp15*$^{lacZ/+}$ gland was sectioned and Eosin-stained to highlight luminal epithelial/myoepithelial-positive cells (scale bars = 500 μm, 1.0 mm, and 50 μm, respectively). (D) qPCR of *Mmp15* at P0, P5 and P10. Results are expressed as mean ± SEM expression levels at P0 (n=4), P5 (n=3) and P10 (n=4) relative to *Arbp*. **p<0.001, *p≤0.01. (E) qPCR of *Mmp14* and *Mmp15* levels in P10 wildtype and *Mmp15*$^{-/-}$ mammary glands. Results are expressed as mean expression levels ± SEM of 3 replicates relative to *Arbp*. **p<0.001. (F) Carmine-stained mammary gland whole mounts

isolated from P0 *Mmp15*$^{+/+}$ and *Mmp15*$^{-/-}$ mice. Ductal penetration (DP) (mm) and total branch point number for P0 *Mmp15*$^{+/+}$ (n=6), *Mmp15*$^{+/-}$ (n=6) and *Mmp15*$^{-/-}$ (n=2) glands are plotted with the mean ± 1 SD. (G) Carmine-stained whole mounts of mammary glands recovered from representative *Mmp15*$^{+/+}$ and *Mmp15*$^{-/-}$ mice at P10. DP and total branch points for P10 *Mmp15*$^{+/+}$ (n=3), *Mmp15*$^{+/-}$ (n=4) and *Mmp15*$^{-/-}$ (n=5) glands are plotted with mean ± SEM. (H) Phase contrast images of mammary epithelial organoids isolated from mice at P10 and embedded within 3-D type I collagen or 3-D Matrigel in the presence of 50 ng/ml FGF-2 (scale bars = 100 μm). P values were calculated with unpaired t-tests. Results are representative of 2 experiments performed.

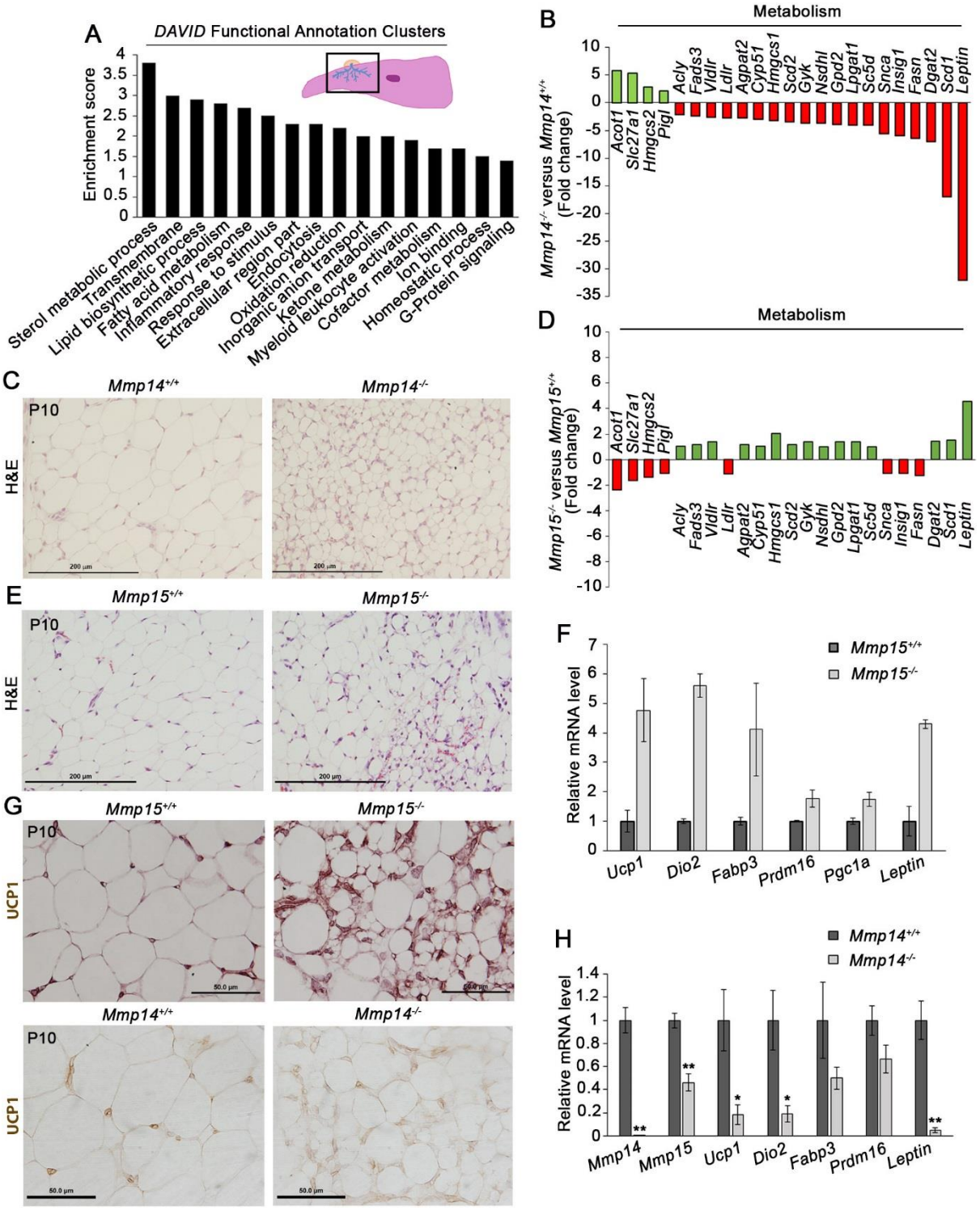

Figure 6. MMP14 and MMP15 differentially regulate mammary fat pad development. (A) Graphical representation of the enriched DAVID Functional Annotation Clusters in P10 *Mmp14*$^{-/-}$ mammary gland tissue relative to *Mmp14*$^{+/+}$ littermates, with a cartoon illustrating the mammary gland region collected for gene expression profiling. (B) Chart of differentially expressed genes related to cellular metabolism in the *Mmp14*$^{-/-}$ gene expression profile, relative to *Mmp14*$^{+/+}$ littermates, plotted by fold change values (n=2 per genotype). (C) H&E staining of fat pad cross-sections from P10 *Mmp14*$^{+/+}$ and *Mmp14*$^{-/-}$ mammary glands. (D)

Chart illustrating the fold-changes in the metabolism genes depicted in panel B in the P10 *Mmp15*$^{-/-}$ gene expression profile relative to *Mmp15*$^{+/+}$ littermates (n=2 per genotype). (E) H&E staining of cross-sections from P10 *Mmp15*$^{+/+}$ and *Mmp15*$^{-/-}$ mammary glands. (F) qPCR of thermogenic and metabolic genes up-regulated in *Mmp15*$^{-/-}$ mammary gland stroma relative to *Mmp15*$^{+/+}$ littermates as normalized to *Arbp*. Results are expressed as mean values ± 1 SD of n=2 mice per genotype. (G) Immunohistochemistry for UCP1 in P10 *Mmp15*$^{-/-}$ and *Mmp14*$^{-/-}$ mammary gland cross-sections with wild-type littermates (scale bars = 200 μm). Results are representative of 3 replicates. (H) qPCR of the genes monitored in panel F in P10 *Mmp14*$^{-/-}$ mammary gland tissue (n=5) relative to *Mmp14*$^{+/+}$ littermates (n=7). Results are expressed as mean expression levels ± SEM as normalized to *Arbp*. **p<0.001, *p<0.05. P values were calculated with unpaired t-tests.

Supporting Information - Figures

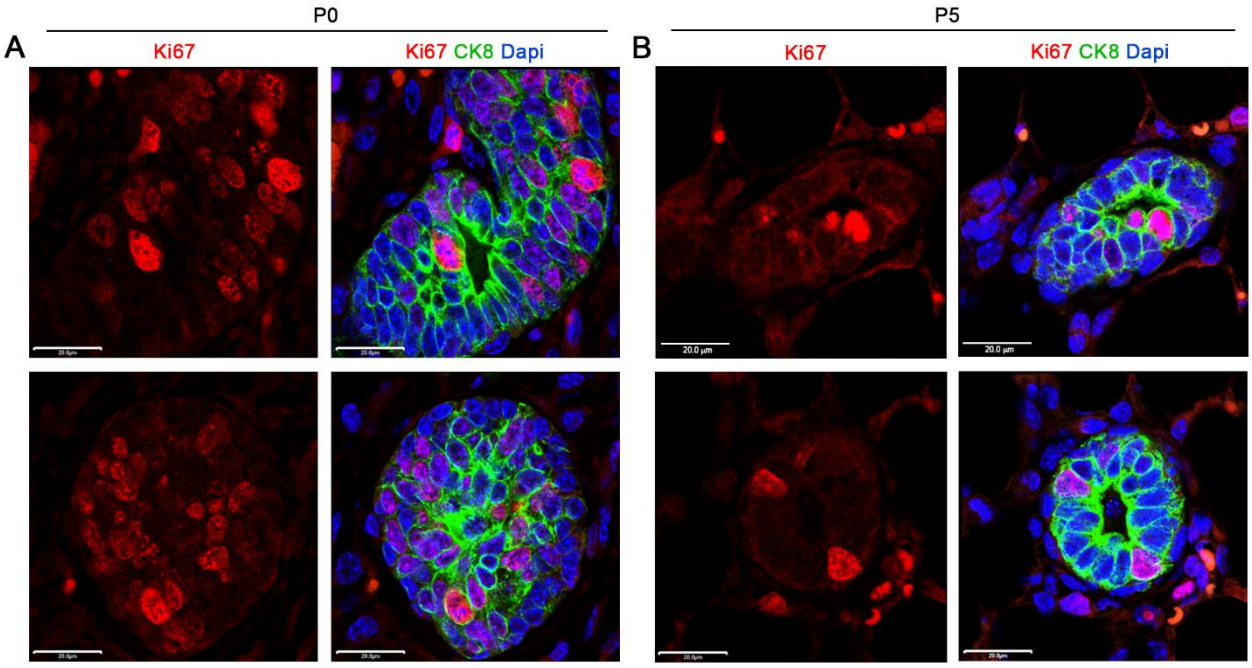

Figure S1. Early postnatal mammary gland morphogenesis coincides with widespread proliferation in the epithelial compartment.

(A,B) Immunofluorescence of Ki67 and CK8 in wild-type P0 (A) and P5 (B) mammary gland cross-sections with DAPI counter-staining (scale bars = 20 µm). Images are representative of 3 replicates.

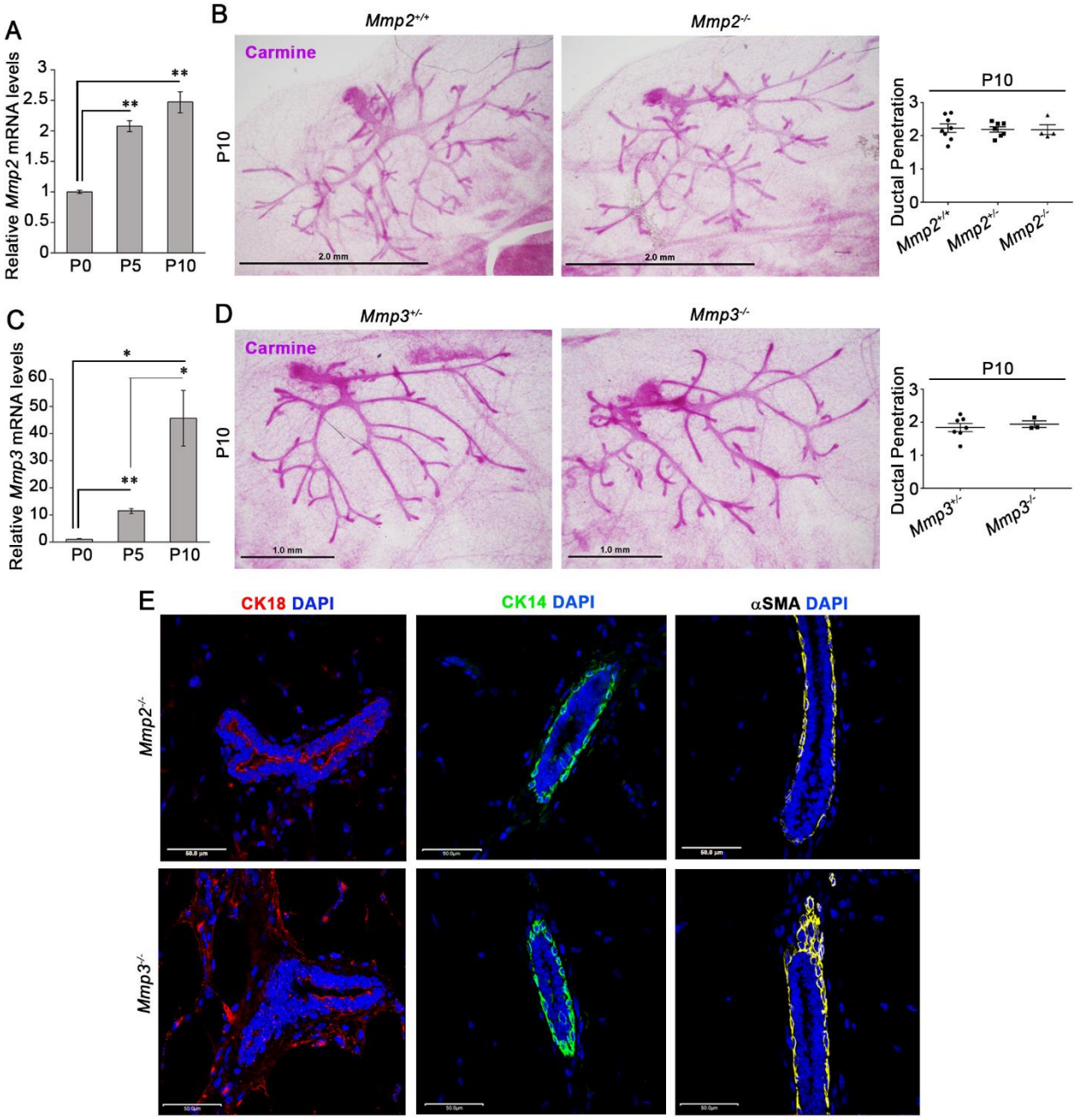

Figure S2. *Mmp2* and *Mmp3* global knockouts establish early postnatal mammary glands. (A) qPCR of *Mmp2* at P0, P5 and P10 in wild-type mammary glands. Results are expressed as mean expression levels ± SEM at P0 (n=4), P5 (n=3) and P10 (n=4) relative to *Arbp*. **p<0.001, *p<0.05. (B) Carmine-stained whole mounts of mammary glands isolated from P10 $Mmp2^{+/+}$ vs. $Mmp2^{-/-}$ mice (scale bar = 2.0 mm) with quantifications of duct penetration (DP) (mm). Results are plotted with mean ± SEM for $Mmp2^{+/+}$ (n=8), $Mmp2^{+/-}$ (n=7)

and *Mmp2*$^{-/-}$ (n=4) mice. (C) qPCR of *Mmp3* at P0, P5 and P10 in wild-type mammary glands. Results are expressed as mean ± SEM for P0 (n=3), P5 (n=3) and P10 (n=4) relative to *Arbp*. **p<0.001, *p<0.05. (D) Carmine-stained whole mounts of P10 mammary glands (scale bars = 1.0 mm) from *Mmp3*$^{+/-}$ mice (n=7) and *Mmp3*$^{-/-}$ mice (n=3) with quantification of DP (mm). Results are plotted with mean ± SEM. (E) Immunofluorescence of CK18, CK14, and αSMA in P10 *Mmp2*$^{-/-}$ and *Mmp3*$^{-/-}$ mammary glands with DAPI counter-staining (scale bars = 50 µm). P values were calculated with unpaired t-tests. Images shown are representative of 2 replicates.

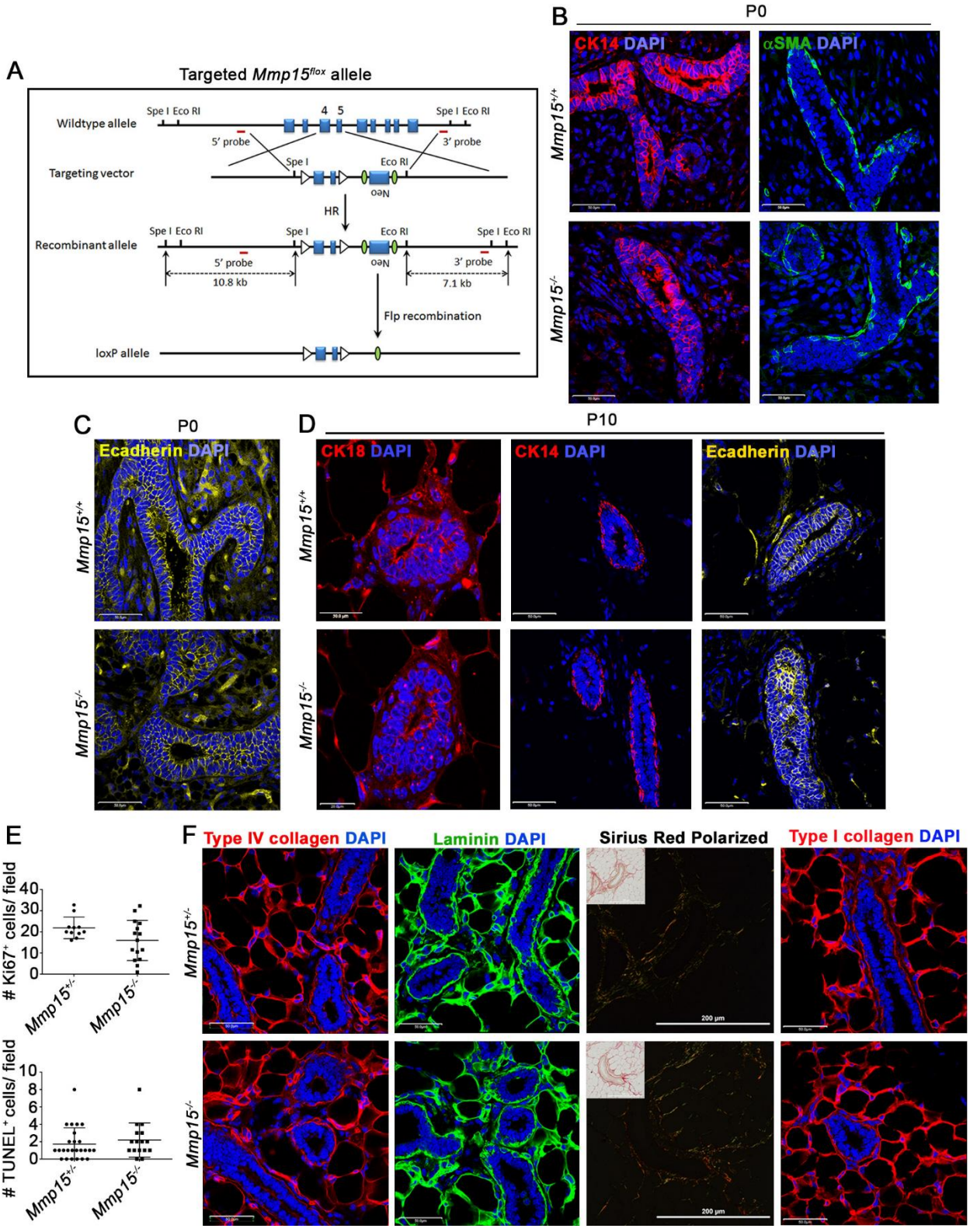

Figure S3. MMP15-independent orchestration of mammary epithelial cell organization, mammary cell proliferation and ECM. (A) Schematic of *Mmp15* global knockout targeting strategy and the *Mmp15*^{flox} allele. (B-C) Immunofluorescence of CK14, αSMA and E-cadherin in P0 *Mmp15*$^{+/+}$ and *Mmp15*$^{-/-}$ mammary glands with DAPI nuclear counter-staining (scale bars = 50 µm). (D) Immunofluorescence of CK18, CK14, and E-cadherin in P10 *Mmp15*$^{+/+}$ and *Mmp15*$^{-/-}$ mammary glands with DAPI counter-staining. (E) Quantification of average number of Ki67-positive cells per field and TUNEL-positive cells per field from immunofluorescence of P5 mammary glands (60X magnification). Results are plotted with mean values of n>10 fields per genotype. (F) Immunofluorescence of type IV collagen, laminin, and type I collagen with DAPI counter-staining in P5 *Mmp15*$^{+/+}$ and *Mmp15*$^{-/-}$ mammary glands (scale bars = 50 µm). Polarized light images of Sirius Red staining of P5 mammary gland cross-sections are also shown. Insets show the corresponding bright-field images (scale bar = 200 µm). All images are representative of n≥2 replicates.

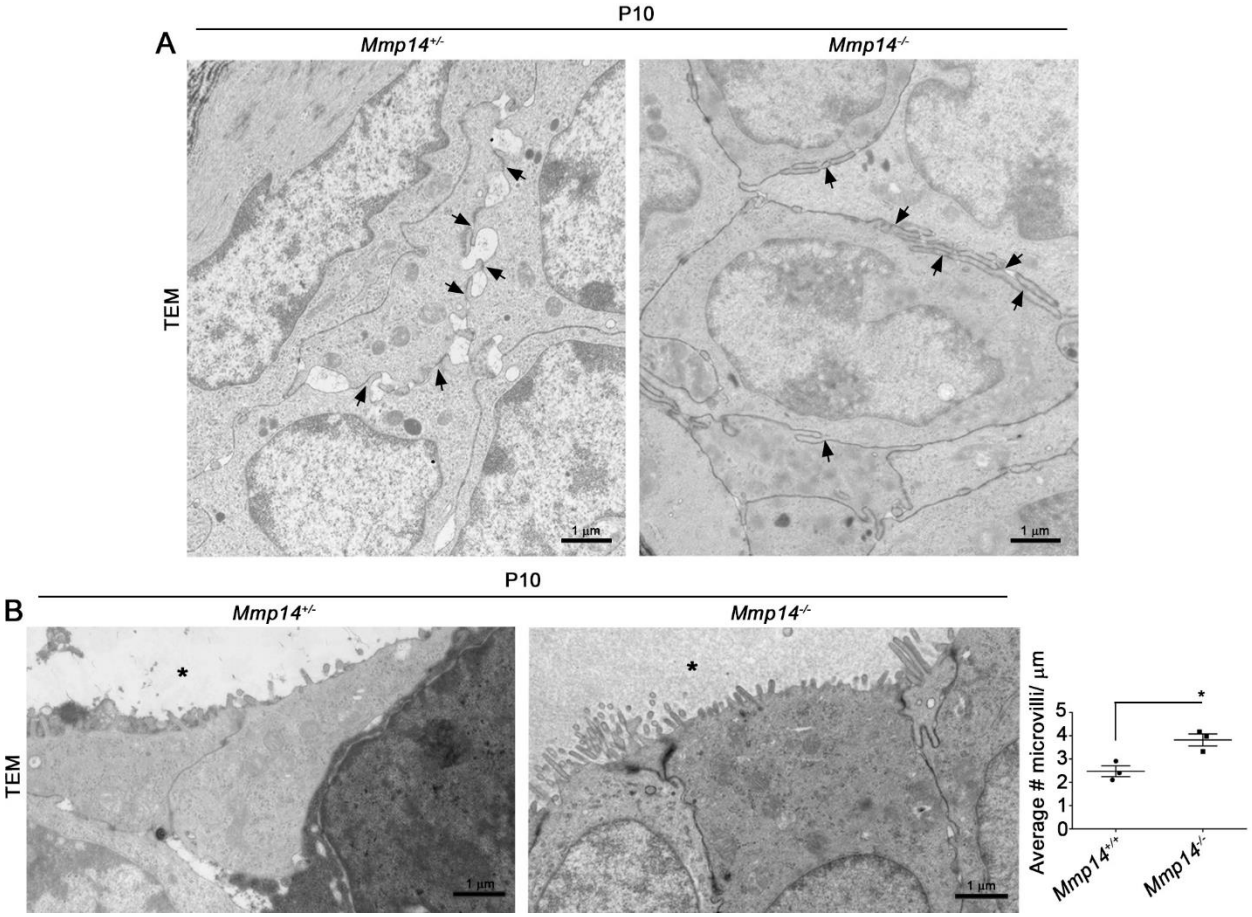

Figure S4. *Mmp14*-dependent regulation of epithelial cell junctions and microvilli *in vivo*. (A) Transmission electron micrographs (TEM) of representative P10 *Mmp14*$^{+/-}$ and *Mmp14*$^{-/-}$ mammary ducts (15000X) (n=3 per genotype). Arrows denote cell-cell junctions and adjacent spaces in *Mmp14*$^{+/+}$ ducts with corresponding regions in *Mmp14*$^{-/-}$ ducts (scale bars = 1 µm). (B) TEM of P10 mammary duct microvilli (15000X) with quantification of average number of microvilli per µm plotted with mean ± SEM (n=3 per genotype). *p<0.02. Asterisks mark the mammary duct lumen (scale bar = 1 µm). P value was calculated with an unpaired t-test.

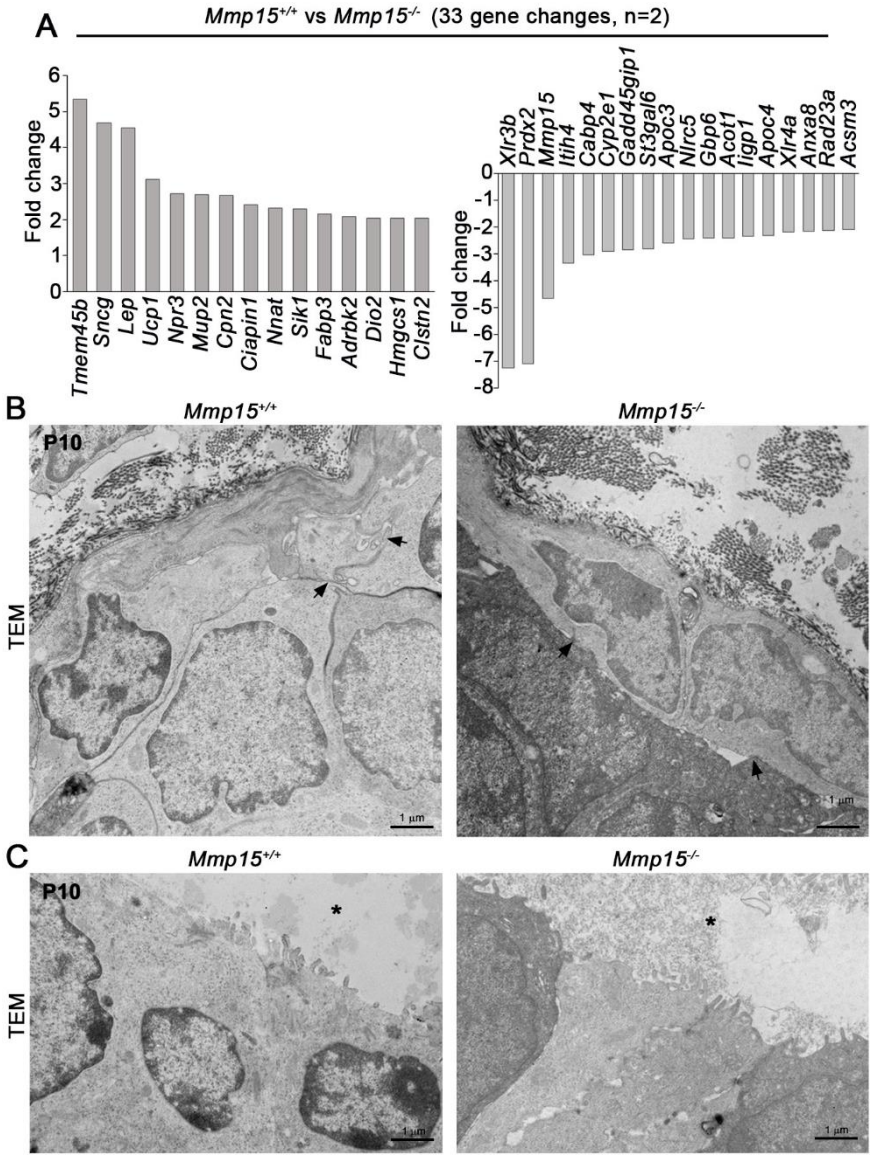

Figure S5. *Mmp15* knockout mammary glands maintain global gene expression profile and epithelial ultrastructure.

(A) Charts of the up-regulated and down-regulated genes in P10 *Mmp15*$^{-/-}$ mammary glands relative to *Mmp15*$^{+/+}$ mammary glands (n=2 per genotype). (B) TEM of representative *Mmp15*$^{+/+}$ and *Mmp15*$^{-/-}$ mammary ducts (15000X) (scale bar = 1 µm). Arrows mark corresponding cell junctions (n=2 per genotype). (C) TEM of representative P10 mammary duct microvilli (15000X) (n=2 per genotype; scale bars = 1 µm). Asterisks mark the mammary duct lumen.

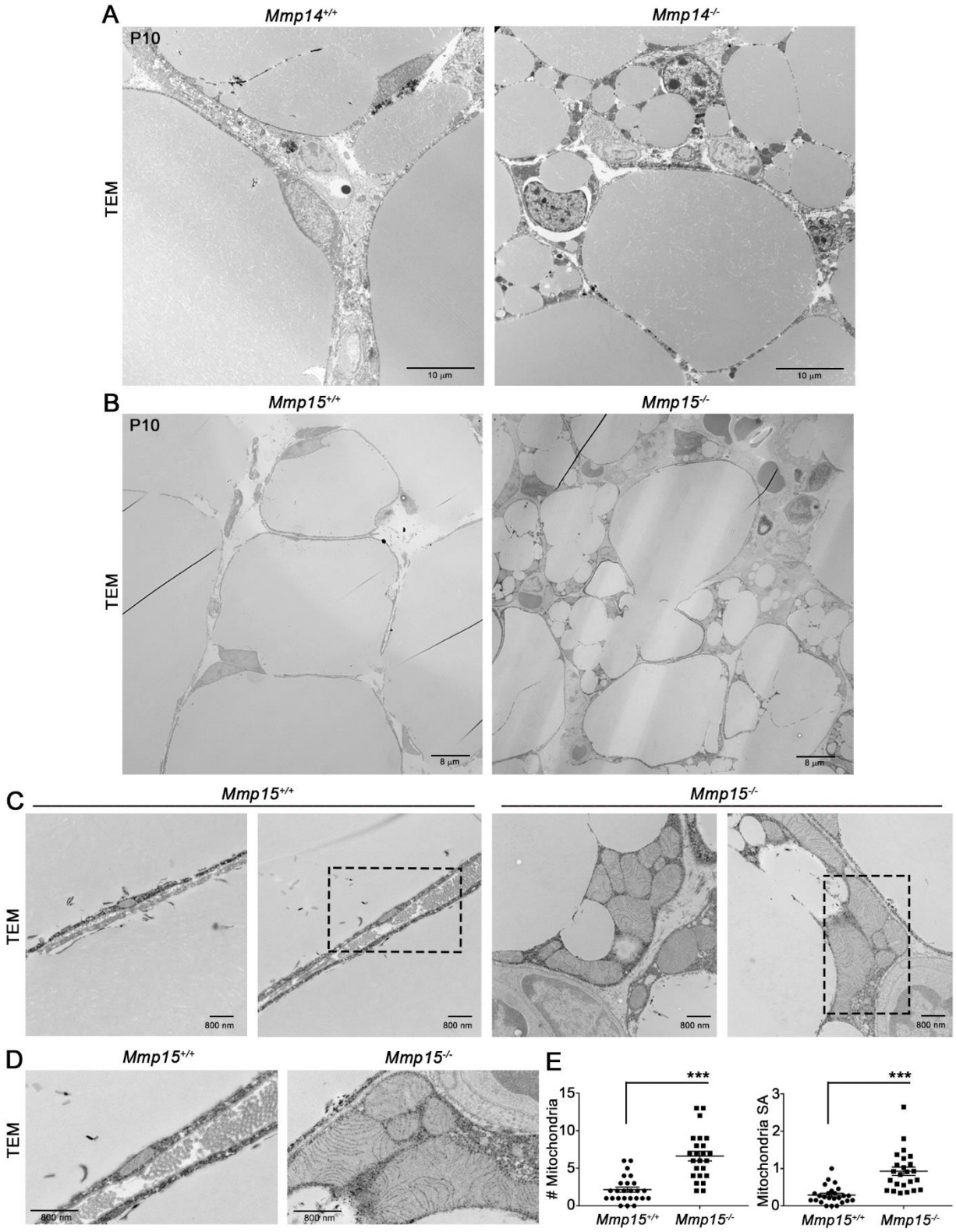

Figure S6. MMP14- and MMP15-dependent regulation of mammary adipocyte development *in vivo.*

(A) Transmission electron micrographs (TEM) of representative P10 *Mmp14*$^{+/-}$ and *Mmp14*$^{-/-}$ mammary adipocytes (1950X, n=3 per genotype, scale bars = 10 µm). (B) TEMs of representative P10 *Mmp15*$^{+/+}$ and *Mmp15*$^{-/-}$ mammary adipocytes (2000X, n=2 per genotype, scale bars = 8 µm). (C) TEMs of representative mitochondria in P10 *Mmp15*$^{+/+}$ and *Mmp15*$^{-/-}$ adipocytes (20,000X, n=2 per genotype, scale bars = 800 nm). Dotted lines circumscribe mitochondria for close-up imaging of cristae (D). (E) Quantifications of mitochondrial number and size (surface area, SA) in *Mmp15*$^{+/+}$ and *Mmp15*$^{-/-}$ TEMs (n=2 mice per genotype, n=25 fields per genotype). ***p<0.00001, as calculated with an unpaired t-test.

Table S1. qPCR Primers

Gene	Forward Primer	Reverse Primer
Gapdh	5'-TGAAGCAGGCATCTGAGGG-3'	5'-CGAAGGTGGAAGAGTGGGAG-3'
Arbp	5'-CACTGGTCTAGGACCCGAGAA-3'	5'-AGGGGGAGATGTTCAGCATGT-3'
Mmp2	5'-TCTGGAGCGAGGATACCCCAA-3'	5'-TTCCAGGAGTCTGCGATGAGC-3'
Mmp3	5'-GTT CCT GAT GTT GGT GGC TT-3'	5'-AGC CTC TCC TTC AGA GAT CC-3'
Mmp15	5'-ACATGTCCACCATGCGCTCT-3'	5'-TACCATGATGTCAGCCTCC-3'
Mmp14	5'-CTGCCATTGCCGCCATGCAAAA-3'	5'-TGGCGTGGCACTCTCCCATACT-3'
Ucp1	5'-AGGCTTCCAGTACCATTAGGT-3'	5'- CTGAGTGAGGCAAAGCTGATTT-3'
Dio2	5'-AATTATGCCTCGGAGAAGACCG-3'	5'-GGCAGTTGCCTAGTGAAAGGT-3'
Fabp3	5'-ACCTGGAAGCTAGTGGACAG-3'	5'-TGATGGTAGTAGGCTTGGTCAT-3'
Prdm16	5'-CCACCAGACTTCGAGCTACG-3'	5'-ACACCTCTGTATCCGTCAGCA-3'
Pgc1a	5'-CCACTTCAATCCACCCAGAAAG-3'	5'-TATGGAGTGACATAGAGTGTGCT-3'
Leptin	5'-GAGACCCCTGTGTCGGTTC-3'	5'-CTGCGTGTGTGAAATGTCATTG-3'

Table S2. Genotyping Primers

Gene	Forward Primer(s)	Reverse Primer	PCR Product Size
Mmp14^{WT}	5'-TAGGCCTGGAACATTCTAACGATC-3'	5'-CTTTGTGGGTGACCCTGACTTGC-3'	900bp
Mmp14^{KO}	5'-TGCGAGGCCAGAGGCCACTTGTGT-3'	5'-CTTTGTGGGTGACCCTGACTTGC-3'	950bp
Mmp14^{lacZ}*(+)*	5'-ACCTGCGTGCAATCCATCTTG-3'	5'-ATGATGGCGGAGGGATCGTTAG-3'	350bp
Mmp14^{lacZ}*(-)*	5'-TGAGGTGGAAAACACGACCAG-3'	5'-ATGATGGCGGAGGGATCGTTAG-3'	180bp
Mmp15^{WT}	5'-CCGCCACCAAGCCTCACTGTCT-3'	5'-AAAGCCACCCACGCCATCAAAC-3'	400bp
Mmp15^{KO}	5'-CGCCACCAAGCCTCACTGTCT-3'	5'-AATTGCTGGGGATGGAGGAAGGTA-3'	470bp
Mmp15^{lacZ}	5'-GAGATGGCGCAACGCAATTAATG-3'	5'-TGCACGTCCCATTCTCATGC-3'	292bp
Mmp2^{WT}	5'-GTGCTACTGCAGGATAAACTGATG-3'	5'-CCGGGACAGGAACGTACTGGGTTC-3'	794bp
Mmp2^{KO}	5'-GCGCCTACCGGTGGATGTGGAATGTGT GCG-3'	5'-CCGGGACAGGAACGTACTGGGTTC-3'	310bp
Mmp3^{WT}	5'-ACCGGATTTGCCAAGACAGAGTG-3'	5'-GCATCTCCATTAATCCCTGGTCC-3'	325bp
Mmp3^{KO}	5'-AGGATCTCCTGTCATCTCACCTTGCTC CTG-3'	5'-AAGAACTCGTCAAGAAGGCGATAGAA GGCG-3'	492bp

Supporting Information - Figures

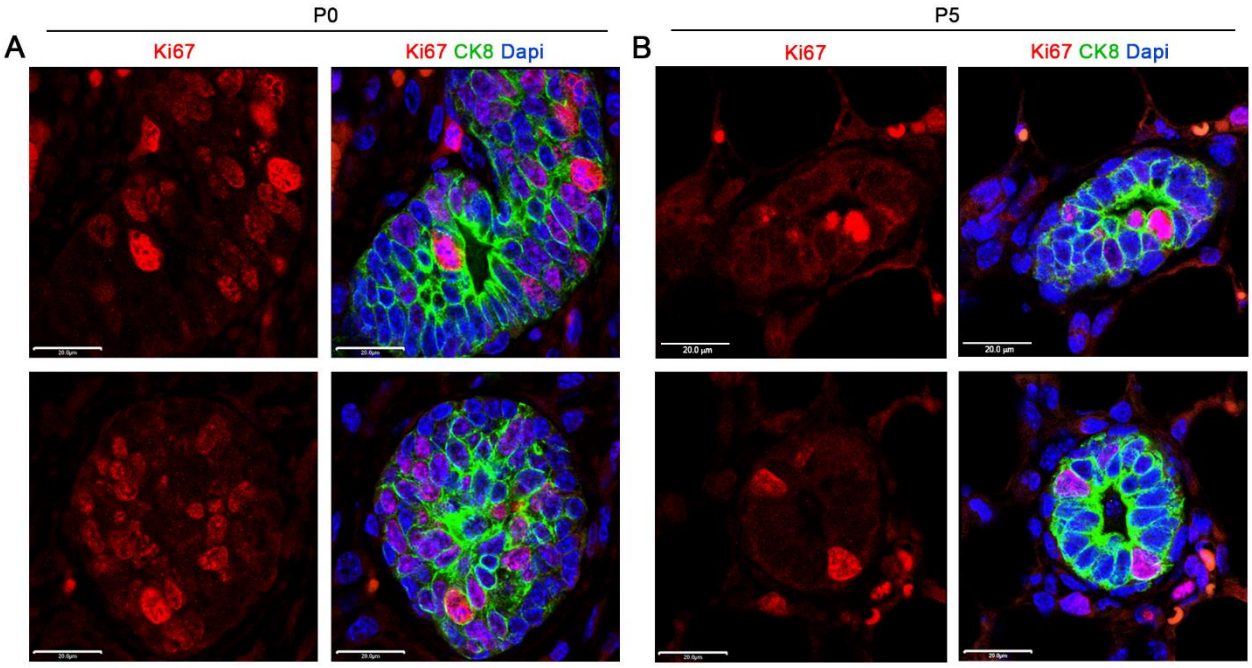

Figure S1. Early postnatal mammary gland morphogenesis coincides with widespread proliferation in the epithelial compartment.

(A,B) Immunofluorescence of Ki67 and CK8 in wild-type P0 (A) and P5 (B) mammary gland cross-sections with DAPI counter-staining (scale bars = 20 µm). Images are representative of 3 replicates.

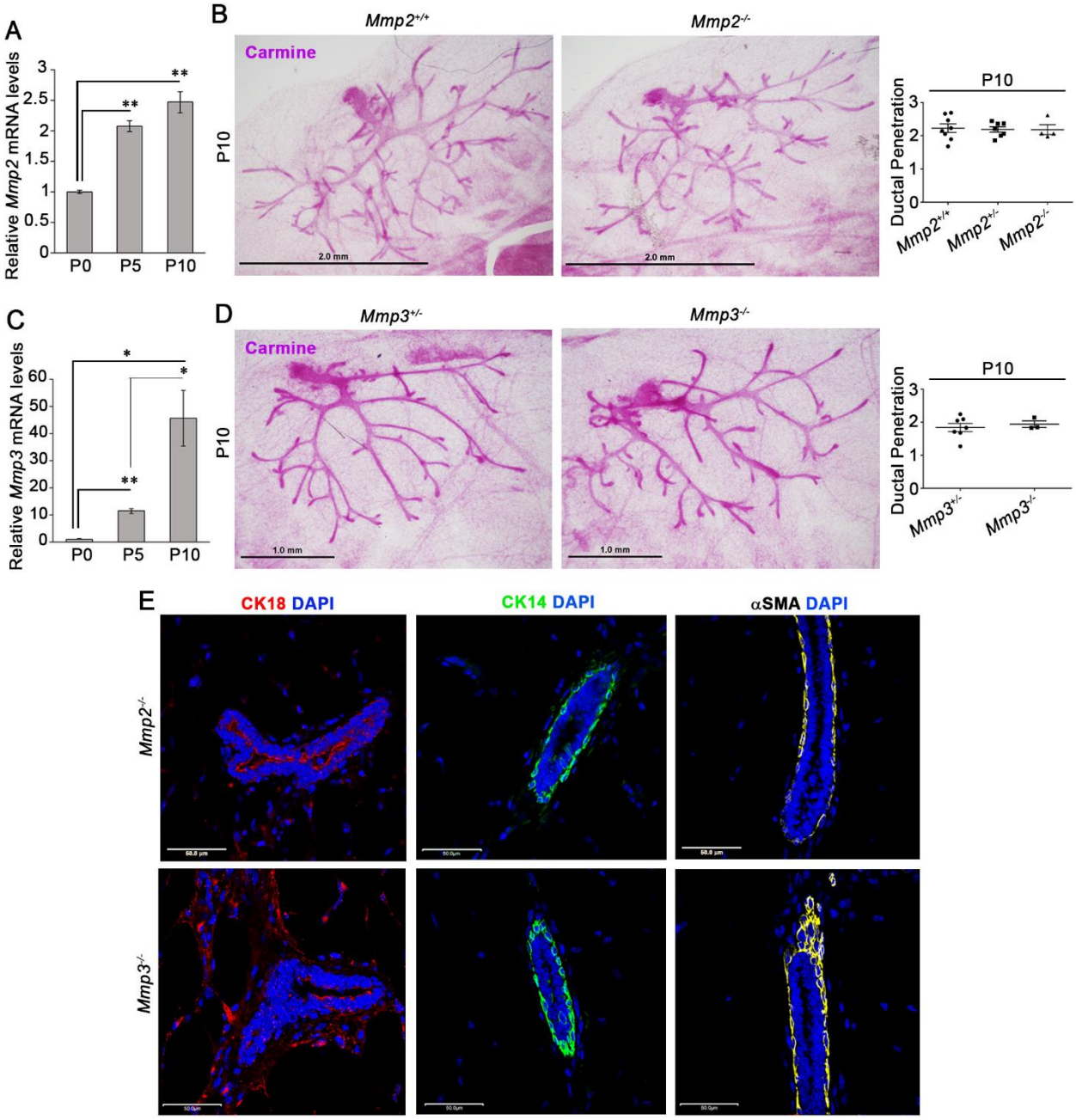

Figure S2. *Mmp2* and *Mmp3* global knockouts establish early postnatal mammary glands. (A) qPCR of *Mmp2* at P0, P5 and P10 in wild-type mammary glands. Results are expressed as mean expression levels ± SEM at P0 (n=4), P5 (n=3) and P10 (n=4) relative to *Arbp*. **p<0.001, *p<0.05. (B) Carmine-stained whole mounts of mammary glands isolated from P10 $Mmp2^{+/+}$ vs. $Mmp2^{-/-}$ mice (scale bar = 2.0 mm) with quantifications of duct penetration (DP) (mm). Results are plotted with mean ± SEM for $Mmp2^{+/+}$ (n=8), $Mmp2^{+/-}$ (n=7)

and *Mmp2*$^{-/-}$ (n=4) mice. (C) qPCR of *Mmp3* at P0, P5 and P10 in wild-type mammary glands. Results are expressed as mean ± SEM for P0 (n=3), P5 (n=3) and P10 (n=4) relative to *Arbp*. **p<0.001, *p<0.05. (D) Carmine-stained whole mounts of P10 mammary glands (scale bars = 1.0 mm) from *Mmp3*$^{+/-}$ mice (n=7) and *Mmp3*$^{-/-}$ mice (n=3) with quantification of DP (mm). Results are plotted with mean ± SEM. (E) Immunofluorescence of CK18, CK14, and αSMA in P10 *Mmp2*$^{-/-}$ and *Mmp3*$^{-/-}$ mammary glands with DAPI counter-staining (scale bars = 50 µm). P values were calculated with unpaired t-tests. Images shown are representative of 2 replicates.

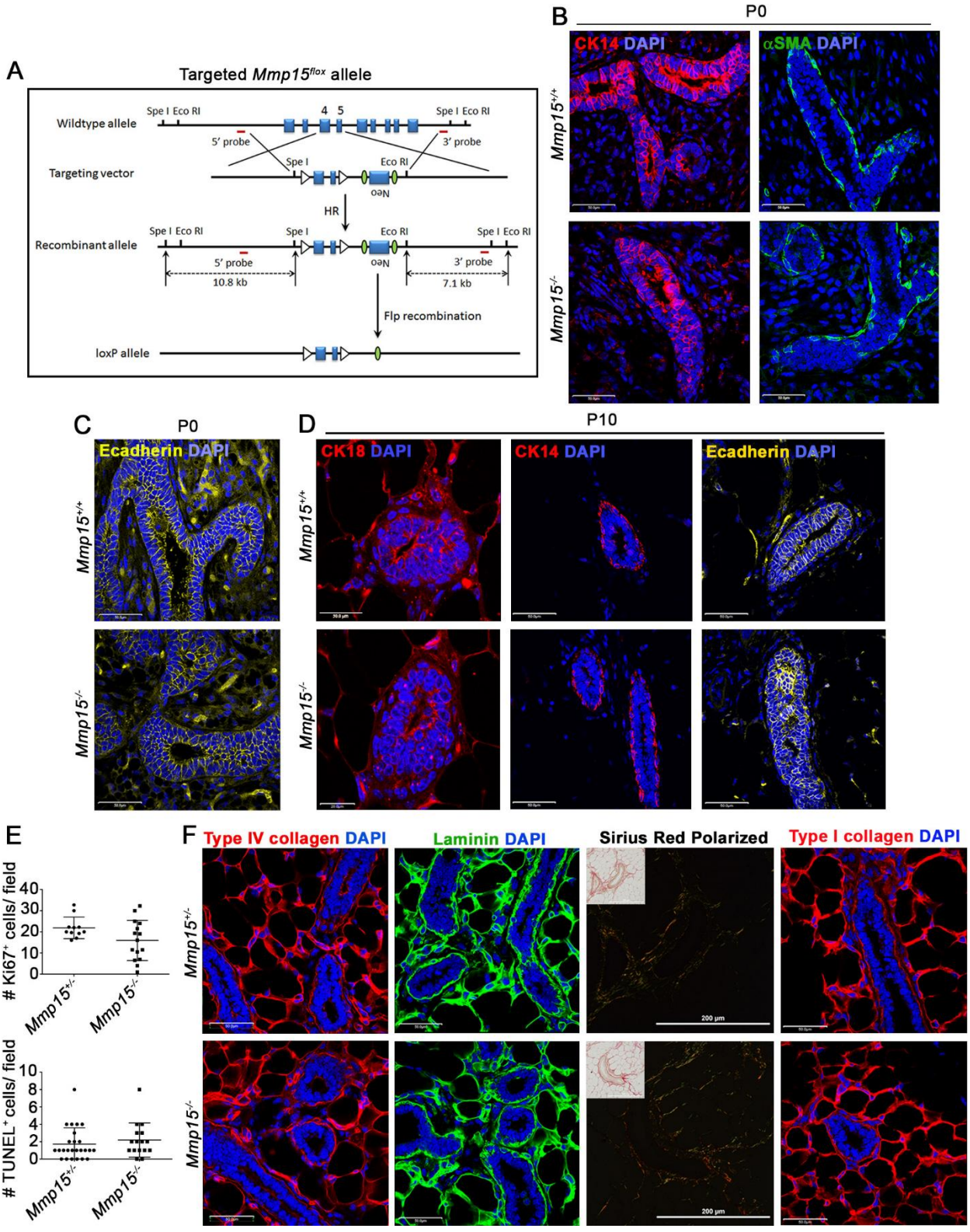

Figure S3. MMP15-independent orchestration of mammary epithelial cell organization, mammary cell proliferation and ECM. (A) Schematic of *Mmp15* global knockout targeting strategy and the *Mmp15*^{flox} allele. (B-C) Immunofluorescence of CK14, αSMA and E-cadherin in P0 *Mmp15*$^{+/+}$ and *Mmp15*$^{-/-}$ mammary glands with DAPI nuclear counter-staining (scale bars = 50 µm). (D) Immunofluorescence of CK18, CK14, and E-cadherin in P10 *Mmp15*$^{+/+}$ and *Mmp15*$^{-/-}$ mammary glands with DAPI counter-staining. (E) Quantification of average number of Ki67-positive cells per field and TUNEL-positive cells per field from immunofluorescence of P5 mammary glands (60X magnification). Results are plotted with mean values of n>10 fields per genotype. (F) Immunofluorescence of type IV collagen, laminin, and type I collagen with DAPI counter-staining in P5 *Mmp15*$^{+/+}$ and *Mmp15*$^{-/-}$ mammary glands (scale bars = 50 µm). Polarized light images of Sirius Red staining of P5 mammary gland cross-sections are also shown. Insets show the corresponding bright-field images (scale bar = 200 µm). All images are representative of n≥2 replicates.

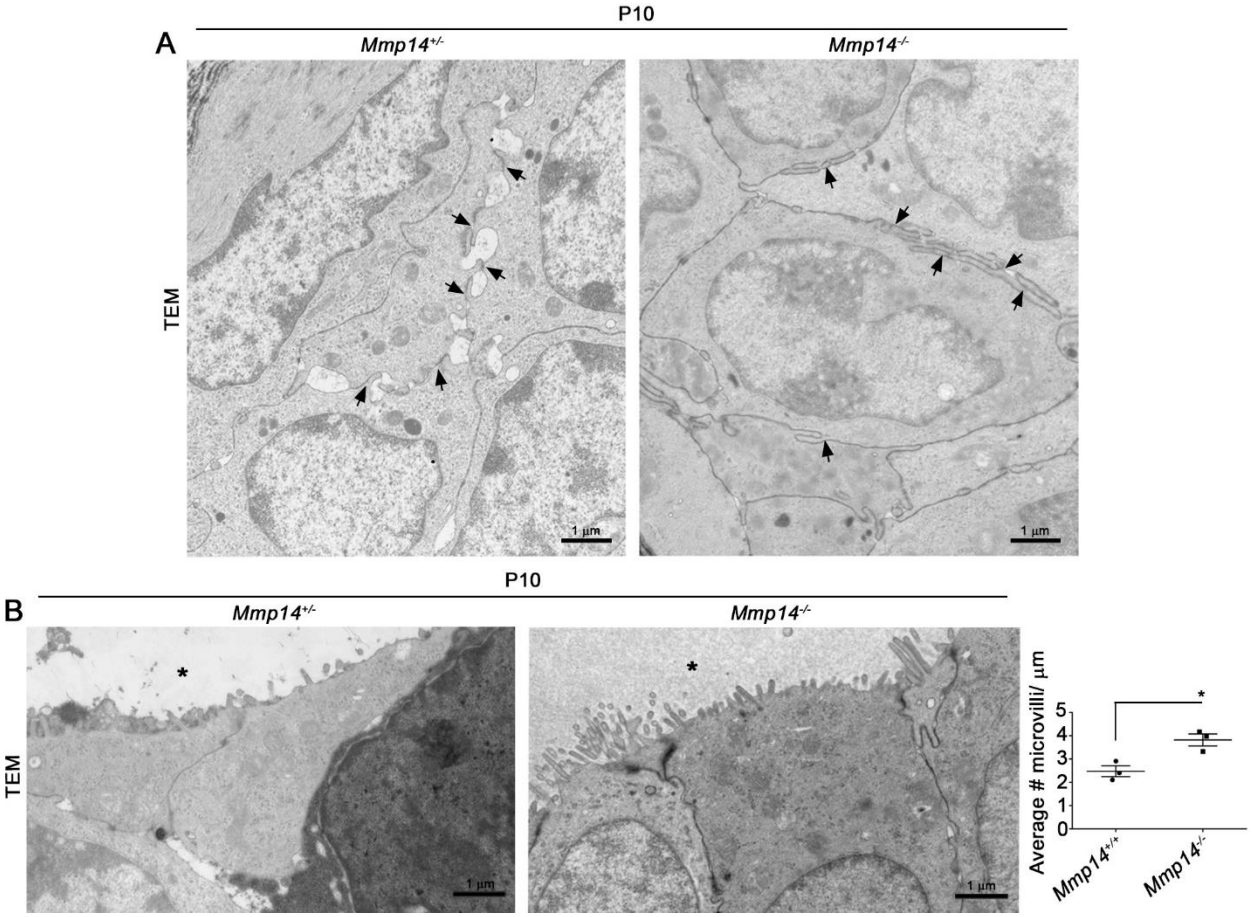

Figure S4. *Mmp14*-dependent regulation of epithelial cell junctions and microvilli *in vivo*. (A) Transmission electron micrographs (TEM) of representative P10 *Mmp14*$^{+/-}$ and *Mmp14*$^{-/-}$ mammary ducts (15000X) (n=3 per genotype). Arrows denote cell-cell junctions and adjacent spaces in *Mmp14*$^{+/+}$ ducts with corresponding regions in *Mmp14*$^{-/-}$ ducts (scale bars = 1 µm). (B) TEM of P10 mammary duct microvilli (15000X) with quantification of average number of microvilli per µm plotted with mean ± SEM (n=3 per genotype). *p<0.02. Asterisks mark the mammary duct lumen (scale bar = 1 µm). P value was calculated with an unpaired t-test.

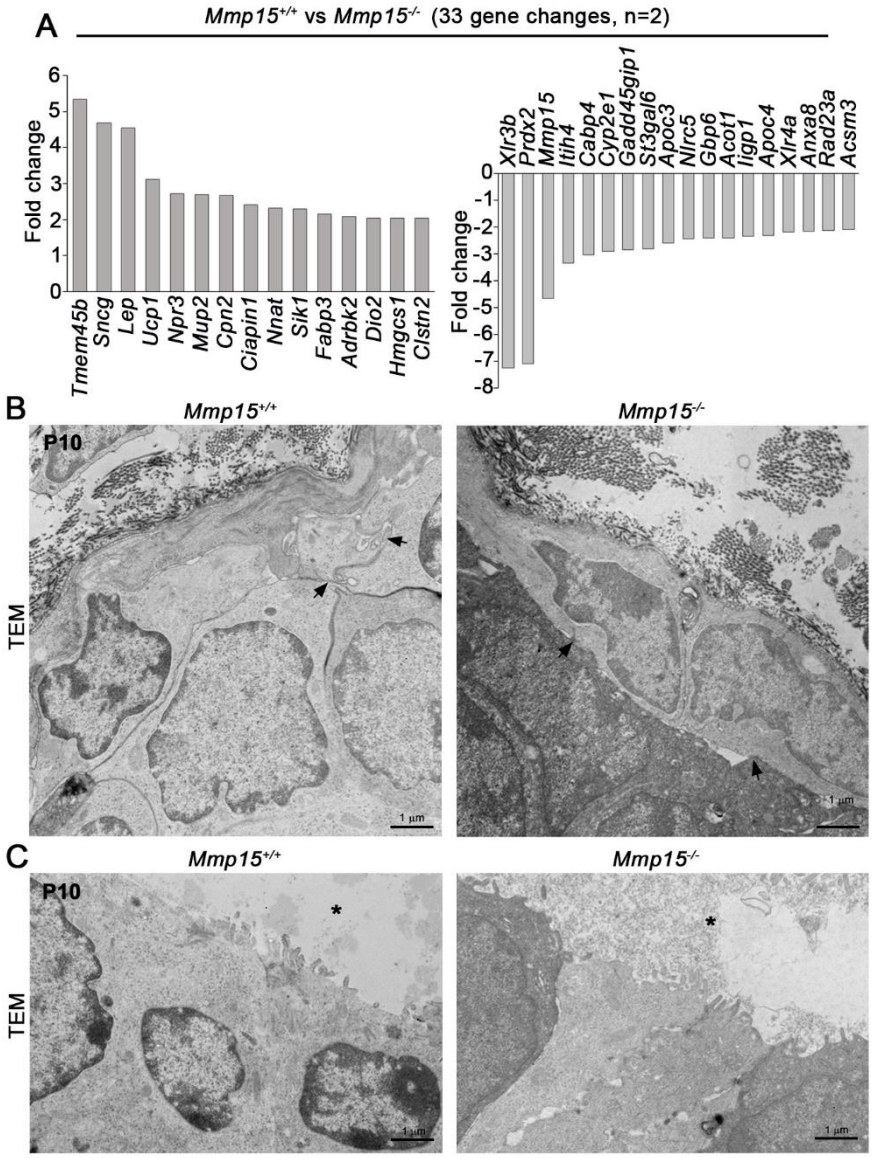

Figure S5. *Mmp15* knockout mammary glands maintain global gene expression profile and epithelial ultrastructure.

(A) Charts of the up-regulated and down-regulated genes in P10 *Mmp15*$^{-/-}$ mammary glands relative to *Mmp15*$^{+/+}$ mammary glands (n=2 per genotype). (B) TEM of representative *Mmp15*$^{+/+}$ and *Mmp15*$^{-/-}$ mammary ducts (15000X) (scale bar = 1 µm). Arrows mark corresponding cell junctions (n=2 per genotype). (C) TEM of representative P10 mammary duct microvilli (15000X) (n=2 per genotype; scale bars = 1 µm). Asterisks mark the mammary duct lumen.

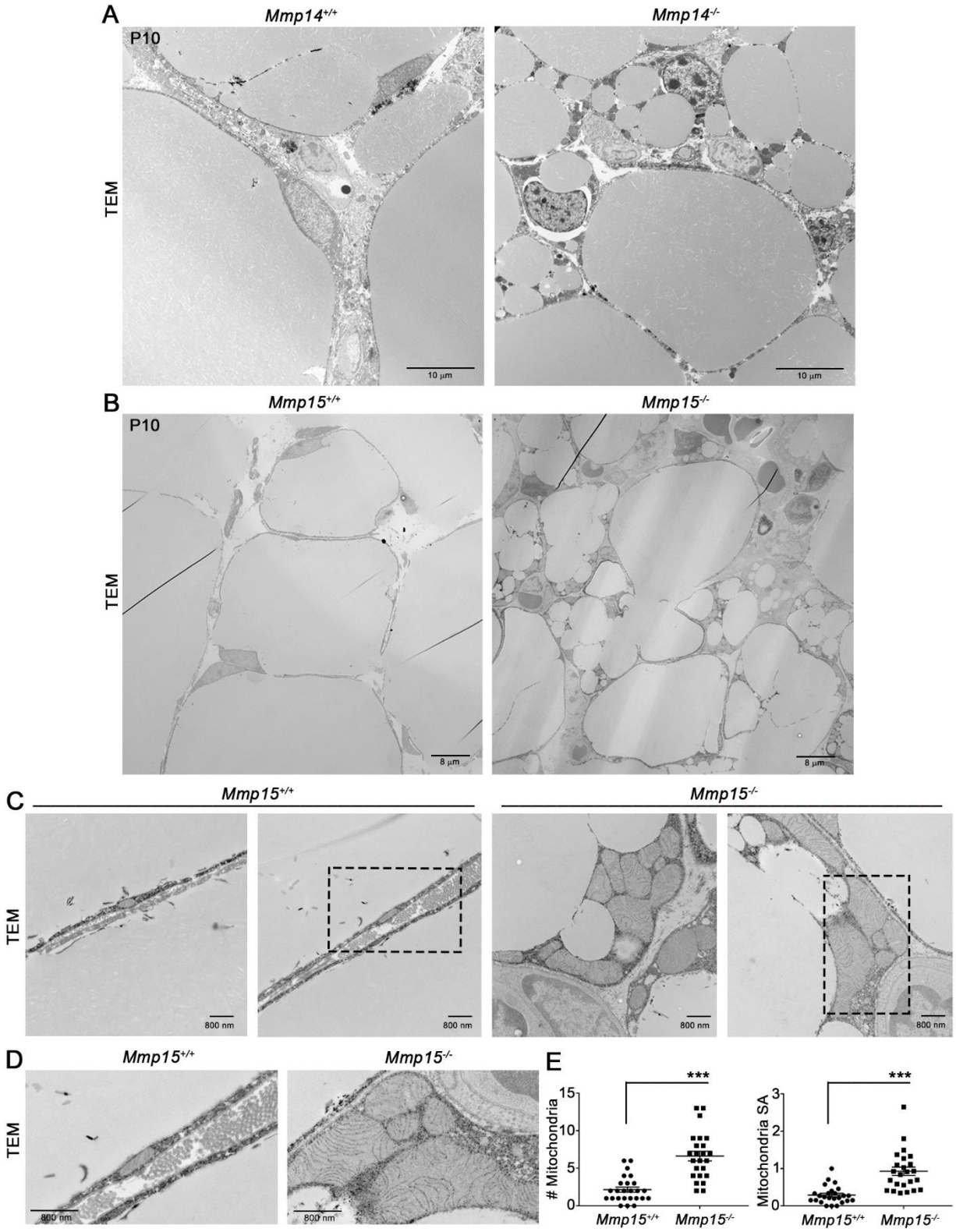

Figure S6. MMP14- and MMP15-dependent regulation of mammary adipocyte development *in vivo.*

(A) Transmission electron micrographs (TEM) of representative P10 *Mmp14*$^{+/-}$ and *Mmp14*$^{-/-}$ mammary adipocytes (1950X, n=3 per genotype, scale bars = 10 µm). (B) TEMs of representative P10 *Mmp15*$^{+/+}$ and *Mmp15*$^{-/-}$ mammary adipocytes (2000X, n=2 per genotype, scale bars = 8 µm). (C) TEMs of representative mitochondria in P10 *Mmp15*$^{+/+}$ and *Mmp15*$^{-/-}$ adipocytes (20,000X, n=2 per genotype, scale bars = 800 nm). Dotted lines circumscribe mitochondria for close-up imaging of cristae (D). (E) Quantifications of mitochondrial number and size (surface area, SA) in *Mmp15*$^{+/+}$ and *Mmp15*$^{-/-}$ TEMs (n=2 mice per genotype, n=25 fields per genotype). ***p<0.00001, as calculated with an unpaired t-test.

Table S1. qPCR Primers

Gene	Forward Primer	Reverse Primer
Gapdh	5'-TGAAGCAGGCATCTGAGGG-3'	5'-CGAAGGTGGAAGAGTGGGAG-3'
Arbp	5'-CACTGGTCTAGGACCCGAGAA-3'	5'-AGGGGGAGATGTTCAGCATGT-3'
Mmp2	5'-TCTGGAGCGAGGATACCCCAA-3'	5'-TTCCAGGAGTCTGCGATGAGC-3'
Mmp3	5'-GTT CCT GAT GTT GGT GGC TT-3'	5'-AGC CTC TCC TTC AGA GAT CC-3'
Mmp15	5'-ACATGTCCACCATGCGCTCT-3'	5'-TACCATGATGTCAGCCTCC-3'
Mmp14	5'-CTGCCATTGCCGCCATGCAAAA-3'	5'-TGGCGTGGCACTCTCCCATACT-3'
Ucp1	5'-AGGCTTCCAGTACCATTAGGT-3'	5'- CTGAGTGAGGCAAAGCTGATTT-3'
Dio2	5'-AATTATGCCTCGGAGAAGACCG-3'	5'-GGCAGTTGCCTAGTGAAAGGT-3'
Fabp3	5'-ACCTGGAAGCTAGTGGACAG-3'	5'-TGATGGTAGTAGGCTTGGTCAT-3'
Prdm16	5'-CCACCAGACTTCGAGCTACG-3'	5'-ACACCTCTGTATCCGTCAGCA-3'
Pgc1a	5'-CCACTTCAATCCACCCAGAAAG-3'	5'-TATGGAGTGACATAGAGTGTGCT-3'
Leptin	5'-GAGACCCCTGTGTCGGTTC-3'	5'-CTGCGTGTGTGAAATGTCATTG-3'

Table S2. Genotyping Primers

Gene	Forward Primer(s)	Reverse Primer	PCR Product Size
Mmp14^{WT}	5'-TAGGCCTGGAACATTCTAACGATC-3'	5'-CTTTGTGGGTGACCCTGACTTGC-3'	900bp
Mmp14^{KO}	5'-TGCGAGGCCAGAGGCCACTTGTGT-3'	5'-CTTTGTGGGTGACCCTGACTTGC-3'	950bp
Mmp14^{lacZ}*(+)*	5'-ACCTGCGTGCAATCCATCTTG-3'	5'-ATGATGGCGGAGGGATCGTTAG-3'	350bp
Mmp14^{lacZ}*(-)*	5'-TGAGGTGGAAAACACGACCAG-3'	5'-ATGATGGCGGAGGGATCGTTAG-3'	180bp
Mmp15^{WT}	5'-CCGCCACCAAGCCTCACTGTCT-3'	5'-AAAGCCACCCACGCCATCAAAC-3'	400bp
Mmp15^{KO}	5'-CGCCACCAAGCCTCACTGTCT-3'	5'-AATTGCTGGGGATGGAGGAAGGTA-3'	470bp
Mmp15^{lacZ}	5'-GAGATGGCGCAACGCAATTAATG-3'	5'-TGCACGTCCCATTCTCATGC-3'	292bp
Mmp2^{WT}	5'-GTGCTACTGCAGGATAAACTGATG-3'	5'-CCGGGACAGGAACGTACTGGGTTC-3'	794bp
Mmp2^{KO}	5'-GCGCCTACCGGTGGATGTGGAATGTGT GCG-3'	5'-CCGGGACAGGAACGTACTGGGTTC-3'	310bp
Mmp3^{WT}	5'-ACCGGATTTGCCAAGACAGAGTG-3'	5'-GCATCTCCATTAATCCCTGGTCC-3'	325bp
Mmp3^{KO}	5'-AGGATCTCCTGTCATCTCACCTTGCTC CTG-3'	5'-AAGAACTCGTCAAGAAGGCGATAGAA GGCG-3'	492bp